VALIDATION OF A LABORATORY METHOD FOR ACCELERATED FATIGUE TESTING OF BRIDGE DECK PANELS WITH A ROLLING WHEEL LOAD

by

Andy Michael Gilbert

A thesis submitted in partial fulfillment
of the requirements for the degree

of

Master of Science

in

Civil Engineering

MONTANA STATE UNIVERSITY
Bozeman, Montana

March 2012

APPROVAL

of a thesis submitted by

Andy Michael Gilbert

This thesis has been read by each member of the thesis committee and has been found to be satisfactory regarding content, English usage, format, citation, bibliographic style, and consistency and is ready for submission to The Graduate School.

Michael Berry

Approved for the Department of Civil Engineering

Dr. Brett Gunnink

Approved for The Graduate School

Dr. Carl A. Fox

STATEMENT OF PERMISSION TO USE

Andy Michael Gilbert

March 2012

ACKNOWLEDGEMENTS

I would like to thank my advisor, Michael Berry, for his encouragement, supervision and useful suggestions throughout this research work. His guidance enabled me to overcome my doubts and complete my work successfully. I am also highly thankful to Dr. Jerry Stephens, Research Director, and Eli Cuelho, Program Manager, for their invaluable support and direction throughout this study. I am grateful for the aid of the Western Transportation Institute for funding my research and education. Without their support, this research would not have been possible. Lastly, I wish to express my appreciation to Zachary Zupan, Adam Stordahl, and Jason Harwood for their contributions.

TABLE OF CONTENTS

TABLE OF CONTENTS - CONTINUED

LIST OF TABLES

LIST OF FIGURES

LIST OF FIGURES - CONTINUED

Figure Page

LIST OF FIGURES - CONTINUED

Figure Page

ABSTRACT

The Western Transportation Institute (WTI) was engaged by the California Department of Transportation (Caltrans) to investigate the performance of various bridge deck rehabilitation surface treatments. This study requires that full-scale reinforced bridge deck slabs be tested in a laboratory environment. The deck slabs are to be tested by applying repeated passes of a rolling wheel load to damage the slabs to certain levels of deterioration. The slabs will be mounted in a frame for testing to impose specific support constraints necessary to generate realistic box girder bridge behavior.

The intent of the present study was to design the panel support frame and validate that it provides the required restraint conditions needed for testing as well as to determine if it will be possible to generate the damage required in future deck slabs in a realistic time frame. This validation was accomplished by performing an experimental study in which a sample test slab was loaded to failure in one of the bays of the support frame. The slab was loaded with a stationary hydraulic jack over a contact area resembling that of a standard dual tire footprint. In addition, the finite element modeling software, ANSYS, was used to model the laboratory test to aid in interpreting the experimental results.

The results from the laboratory test and the related findings from the finite element model were presented in terms of cracking behavior, deflection histories, strain measurements in the steel reinforcement, ultimate capacity, and mode of failure. The results were used in conjunction with the finite element model to validate the performance of the support frame. It was determined that the support frame provides the restraint conditions needed to create the in-service stress conditions of interest in the bridge deck slabs. A fatigue life model that was developed by past researchers was used to assess the expected performance of the deck specimens under the proposed rolling wheel loads.

CHAPTER 1 - INTRODUCTION

Background

The California Department of Transportation (Caltrans) currently performs inspection and maintenance on more than 12,300 state highway bridges, half of which are older than 40 years (Rahim et al., 2006). The most common type of distress observed in these bridges is deck cracking. Bridge deck cracks are primarily found in the direction transverse to the main bridge span. Transverse cracking accelerates corrosion of the reinforcing steel, deteriorates the deck concrete, and reduces the life-span of the bridge. In California, the bridge repair costs due to reinforcement corrosion alone are estimated to be 200 million dollars a year (Pan et al., 2007). The repair work is complicated by California's predominant usage of box girder bridges. In their box girder bridges, the structural deck is the top flange of the box girder, which makes for difficult removal of the deck when deck replacement is deemed necessary. As an alternative to bridge deck replacement, Caltrans like many other states, employs a rehabilitative approach of applying surface treatments to the bridge decks.

The Western Transportation Institute (WTI) has been engaged by Caltrans to validate the long term effectiveness of five rehabilitation surface treatments: high molecular weight methacrylate (HMWM) sealant, polyester overlay with partial deck removal, polyester overlay without deck removal, Portland cement overlay, and asphalt concrete overlay. The main objective of the study is to investigate the performance of each rehabilitation method over the useful life of a bridge deck. This performance is influenced by the condition of the deck when the treatment is applied. Thus, to realize

the project objective, decks exhibiting various levels of distress need to be treated, and then further distressed to failure.

In light of the complexities of the system to be studied, WTI was tasked with developing a test program that incorporates the level of control offered in laboratory rather than field testing, coupled with the level of confidence provided by testing actual bridge deck panels. In order to accomplish this objective, the decision was made in consent with Caltrans that full size panels need to be tested under a rolling wheel load in the laboratory. The samples will be fatigued by the rolling wheel load to certain levels of deterioration, at which time they will be rehabilitated, and fatigue testing will then resume.

Following this strategy, WTI's research team recommended that flat deck panels that are 8 feet 5 ½ inches long in the direction of wheel travel, 7 feet wide in the transverse direction, and 6.5 inches thick be tested (see Figure 1). The reinforcement arrangement will be consistent with California standard practices. The samples will be tested in a support frame designed to simulate continuity conditions in actual bridges by providing fixed-fixed boundary conditions (rotation and vertical translation restraint) along the longitudinal edges of the deck specimens, as depicted in Figure 1. The support frame was also designed to provide simple support of the leading and trailing edges of the samples to eliminate large and unrealistic stress conditions associated with the alternative of a free edge. This laboratory testing configuration was thought to replicate the transverse behavior of the top surface of a box girder bridge under rolling wheel loads.

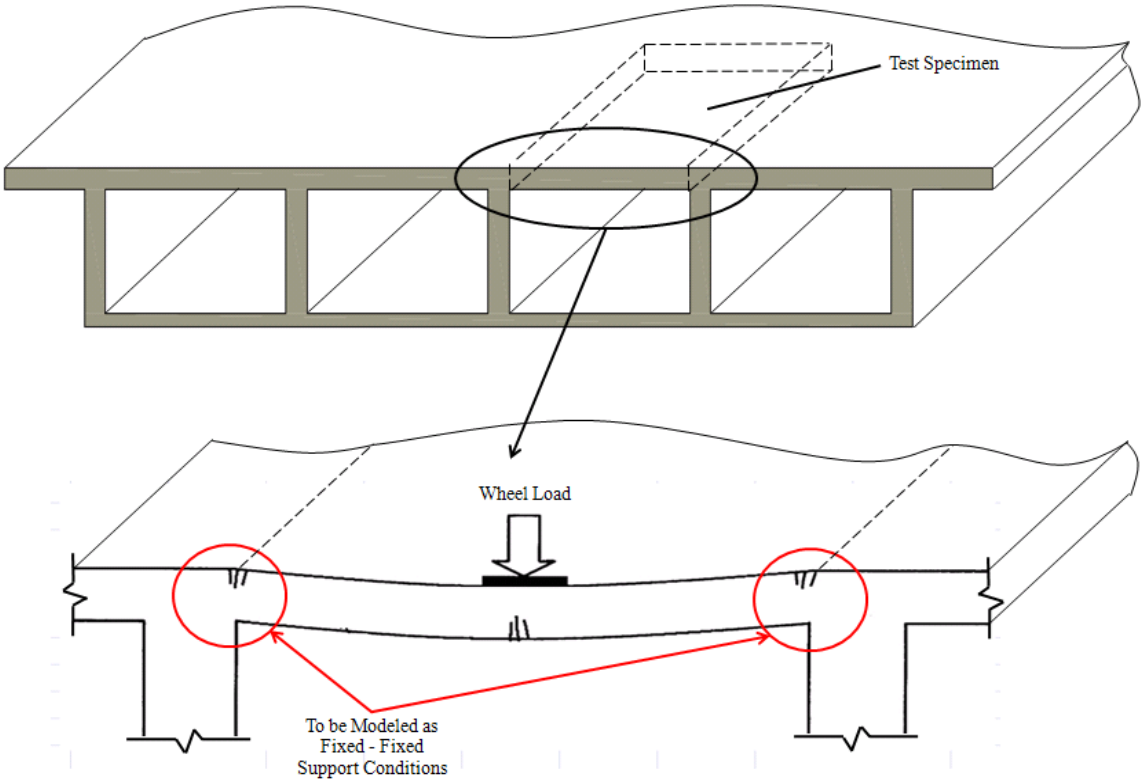

Figure 1: Continuity Conditions in a Deck Element of a Box Girder Bridge

Objectives and Scope

The specific objective of the present study was to design the deck panel support frame and then validate its expected performance in testing full-scale bridge deck models under a rolling wheel load. More specifically, this research verified that the as designed and constructed deck panel support frame provides the restraint conditions needed for fatigue testing of the deck panels under in-service conditions. Design of the testing frame was done with the assistance of a solid material based finite element modeling package (ANSYS, 2008). The support frame was then built by a commercial fabrication shop and assembled in the laboratory. Frame performance was evaluated by statically loading to

failure a typical bridge deck specimen that was mounted in the support frame. Further, a non-linear reinforced concrete finite element model was built in ANSYS to provide a valuable supplement to the physical investigation of the frame performance and panel response. The results of the static load test were then used in a modified fatigue life model to predict the number of load cycles (applied by a rolling wheel load) required to deteriorate a bridge deck specimen once testing begins. These predictions were used to determine the practicality of generating required deterioration levels in the test panels in a reasonable amount of time.

Outline

This thesis is organized into five chapters. The first chapter provides an introduction to the study and its objectives. Chapter 2 includes the results of the literature search that was conducted throughout the course of this research. Chapter 3 describes the methods used in the design of the test panel support frame and conduct of both the static load test and finite element analysis. The analysis and discussion of the results from the experimental study and finite element model are presented in Chapter 4. Chapter 5 provides a summary of the conclusions and recommendations for future research. Lastly, detailed information on the configuration of the test panel and test frame (including fabrication drawings) is presented in Appendix A.

CHAPTER 2 - LITERATURE REVIEW

Introduction

To present a comprehensive review of all the literature relevant to concrete bridge deck distresses and rehabilitation strategies is impractical and beyond the scope of this thesis. This review focuses on past contributions most closely related to the needs of the current project, notably, reproducing in the laboratory realistic structural behaviors of full size, in-service bridge decks. A laboratory methodology for static testing of full-scale bridge deck models is discussed inclusive of predicted results for fatigue testing with rolling wheel loads. Finite Element Modeling (FEM) of reinforced concrete is explained as a prelude to the modeling done for this specific part of the project.

Laboratory Methods for Testing Full-Scale Bridge Deck Models

Extensive testing has been done on full-scale bridge deck models; however, El-Gamal et al. (2005) was the first to test full-scale slabs in a frame (described below) that was thought to be an economical alternative to the approach used by past researchers including Newhook (1997) and Khanna et al. (2000), whereby slab restraint was provided by monolithically casting the deck panels on the supporting steel beams of the frame, with welded steel studs anchoring the deck to the beams. El-Gamal (2005) and his colleagues were performing static load tests to study the behavior of concrete bridge decks reinforced with fiber reinforced polymer (FRP) bars. Each deck slab was tested to failure using a monotonically applied, concentrated load. The load was applied over a specified contact area to simulate the footprint of a standard truck wheel load acting on

the center of the slab. The experimental results that were presented included: cracking profiles, load deflection responses, strain histories in the concrete and reinforcement, ultimate capacity, and mode of failure for each slab. In a similar study conducted by El-Ragaby et al. (2007), full-scale models of bridge deck slabs were tested to investigate the fatigue life of decks reinforced with FRP bars. The deck slabs were pre-cracked and then tested under concentrated cyclic loading until failure. A fatigue-life prediction model was generated based on the experimental test results.

In the tests done by both El-Gamal et al. (2005) and El-Ragaby et al. (2007), the test slabs were approximately 10 feet long, 8 feet wide, and 8 inches thick. The width and thickness dimensions were chosen to represent common bridge decks in Canada, while the length dimension was selected to include the area that would be affected by a punching shear failure. In both tests, one of the test slabs was reinforced with conventional steel, and the remaining slabs were reinforced with varying amounts of FRP reinforcement in the transverse direction.

The testing frame developed by El-Gamal et al. (2005) and later used by El-Ragaby et al. (2007) was intended to restrain full-scale bridge deck models from rotation and vertical translation along their longitudinal edges. Thus, this testing frame was to provide the edge restraint within the test specimens needed to simulate field conditions. As seen in Figure 2, each bridge deck specimen was supported on two stiffened, steel, wide flange beams. Both longitudinal edges of the deck slab were bolted to the top flange of a support beam through two rows of holes using structural steel bolts and a steel restraint channel. All of the bolts were pre-tensioned to the same level of torque to

provide an equal and uniform edge clamping force. Also, neoprene pads were used at all interfaces between the steel sections and the deck slab. Three evenly spaced steel cross frames were used to provide lateral support within the testing frame.

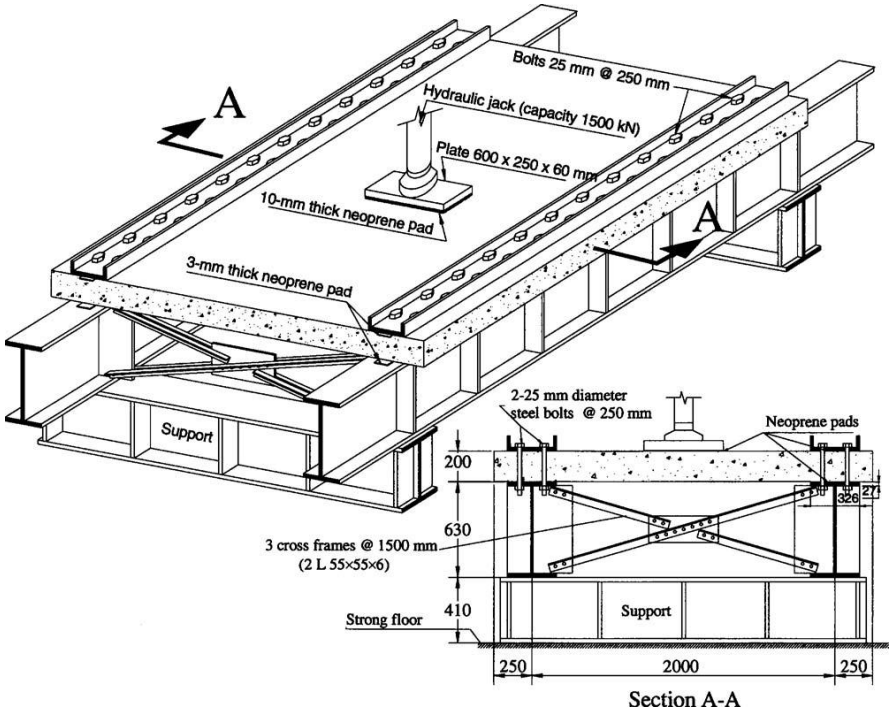

Figure 2: Isometric View and Cross Section of Testing Frame (El-Gamal et al., 2005)

El-Gamal et al. (2007) verified that the deck panel support system provided restrained conditions based on their results from statically testing four full size test specimens. The observed crack patterns and the measured displacements within the deck slabs indicated that that the expected distribution of flexural stresses existed within the slabs. These flexural stresses included transverse tensile stresses in the top of the deck near the face of the supports, and compressive stresses in the top surface at the mid-span.

Only minimal strains were measured in the intermediate cross frame, indicating that the cross frames were not needed within the testing frame.

El-Gamal et al. (2005) and El-Ragaby et al. (2007) used similar instrumentation in testing their bridge deck panels. For each test specimen, resistance strain gauges were used to measure strain in the top and bottom reinforcing bars and on the top surface of the concrete around the loaded area. In the tests done by El-Gamal et al. (2007), strain was also measured within the testing frame. Multiple Linear Variable Displacement Transducers (LVDTs) were used to measure deflections in the test slab at different locations around the loaded area and at the supporting girders. All of the readings of the strain gauges, LVDTs, and the load cell were recorded using a computer monitored data acquisition system.

Predicted Results for Fatigue Testing with Rolling Wheel Loads

A considerable amount of research has been done on fatigue testing full-scale bridge deck slabs. Most work, however, has been done using stationary pulsating loads rather than moving wheel loads. Perdikaris and Beim (1988) performed both pulsating load and rolling wheel load tests on scale models of reinforced concrete slabs. Their tests revealed that the moving wheel load produced far more damage in the concrete slabs than the fixed pulsating load. This significant reduction in fatigue life for moving wheel loads was also reported in work done by Gebreyouhannes et al. (2008). Similar work using moving wheel loads on scale slab models was done by Petrou et al. (1994), where it was observed that if the applied load on the slab was slightly below the cracking load, the

slab's fatigue life was estimated to be up to 40 times greater than if it were loaded at the cracking load.

Matsui et al. (2001) were the first to test full-size bridge deck slabs under a moving wheel load. The tests were conducted on 7-inch thick, simply supported, reinforced concrete slabs and led to the development of the following fatigue life (P - N) relationship:

$$\log \frac{P}{P_s} = -0.07835 \log(N) + \log(1.52)$$

Equation 1

where, P is applied load, P_s is the punching shear capacity of the deck slab, and N is number of cycles to failure. The equation was reported to be valid only for values of N greater than 10,000 cycles. Since the relationship was based on tests on full-scale specimens and was reported to be valid for different types of concrete bridge deck slabs, El-Ragaby et al. (2007) made an effort to verify this fatigue life model. Based on their fatigue tests on full-scale slabs reinforced with FRP's, El-Ragaby et al. (2007) developed the following fatigue life equation to compare to that of Matsui et al. (2001):

$$\frac{P}{P_s} = 0.0034(\log N)^2 - 0.11873(\log N) + 1.0752$$

Equation 2

As seen in Figure 3, the fatigue life relationships are in good agreement for values of N greater than 10,000 cycles.

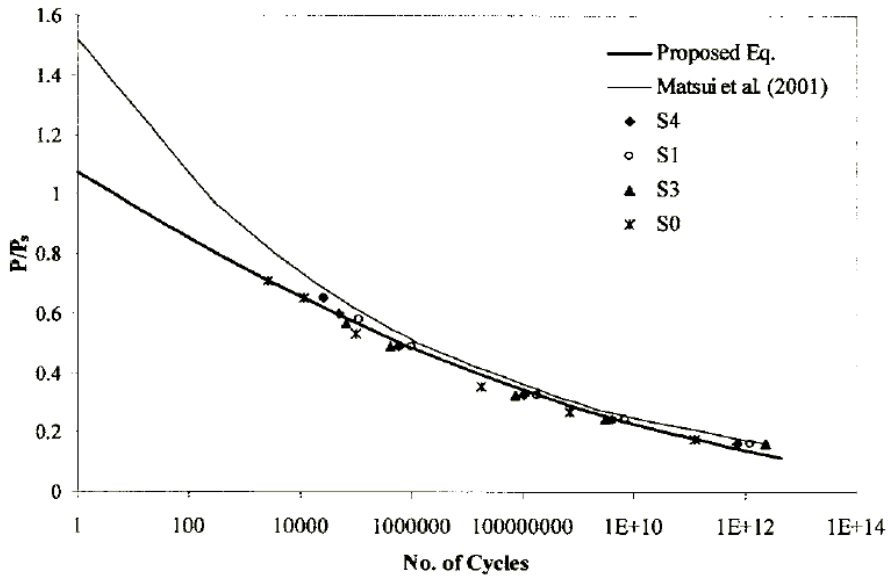

Figure 3: Fatigue Life Curves for Full-Scale Concrete Bridge Decks (El-Ragaby et al., 2007)

In both of the fatigue life curves shown, the ultimate static strength of the deck slabs were assumed to be the punching shear capacities of the slabs. This assumption was verified by Graddy et al. (2002) who investigated the punching shear behavior of bridge decks under fatigue loading. Graddy et al. (2002) established that the predominant failure mode for concrete bridge decks tested using static, pulsating, or moving wheel loads is punching shear and not flexure.

Predicting Punching Shear Capacities of Restrained Bridge Deck Slabs

In order to use the fatigue life models for reinforced concrete bridge decks developed by both Matsui et al. (2001) and El-Ragaby et al. (2007), an accurate estimate of the slabs punching shear capacity is required. This parameter can be obtained from experimental data and from predicted capacity equations. Both the American Association

of State Highway and Transportation Officials (AASHTO) and the American Concrete Institute (ACI) provide code equations for predicting the punching shear capacity of concrete slabs. However, in work done by Kuang and Morley (1992), the code equations were found to be inaccurate in predicting capacities of restrained concrete slabs. Kuang and Morley (1992) performed punching tests on 12 one-fifth scale reinforced concrete deck slabs. In all tests, the punching shear capacities were significantly higher than those predicted by AASHTO and ACI equations. It was concluded that the code predictions do not take into account the compressive membrane forces that develop in the slab specimens due to the translational restraint provided by the testing frame along the edges of the slab. This conclusion was also confirmed by other past research (Fenwick and Dickson, 1989; Mufti and Newhook, 1998; Graddy et al., 2002; Salim and Sebastian, 2003).

The following are general equations used for predicting the punching shear capacity of non-pre-stressed reinforced concrete slabs being loaded with a rectangular footprint (Graddy et al., 2002):

$$V_c = 2\left(b_1 + b_2 + \frac{2d}{\tan\theta}\right)\frac{d}{\tan\theta} f_t$$

Equation 3

$$f_t = \left(2 + \frac{4}{b_2 / b_1}\right)\sqrt{f'_c} \leq 4\sqrt{f'_c}$$

Equation 4

where V_c is the punching shear capacity (lb.), b_1 is the short side of the concentrated load (in.), b_2 is the long side of the concentrated load (in.), d is the average effective depth (in.), θ is the acute angle between the horizontal and the assumed failure plane (degrees), f_t is the diagonal tensile strength of the concrete (psi), and f'_c is the specified compressive strength of the concrete (psi). The equation is derived from equilibrium of forces acting on the assumed failure planes shown in Figure 4.

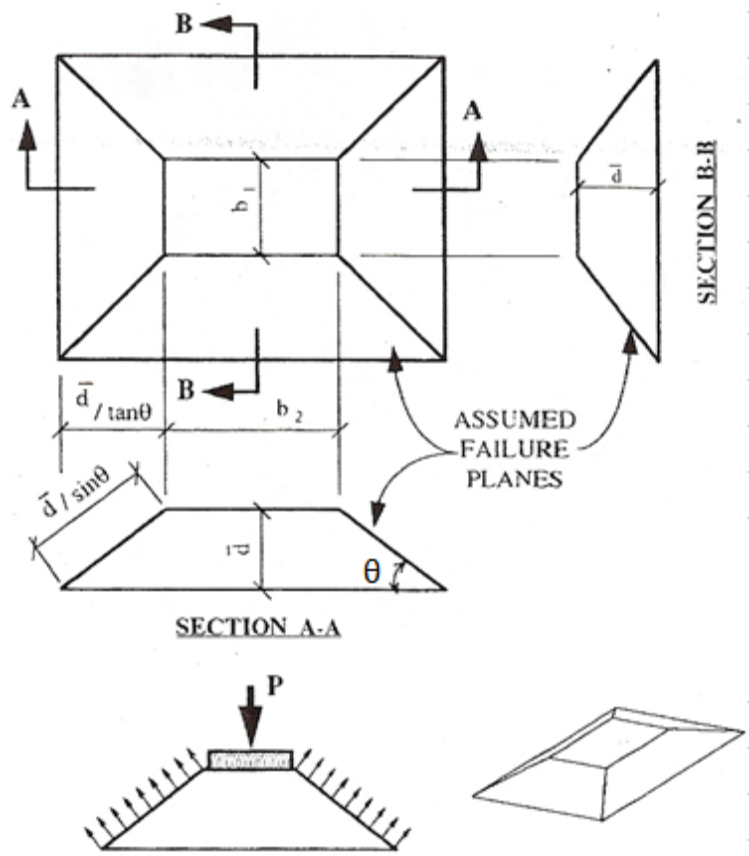

Figure 4: Assumed Failure Planes and Acting Forces for General Punching Shear Model (Graddy et al., 2002)

The general punching shear equation reduces to the AASHTO and ACI equations for predicting punching shear capacities when the angle θ is set to 45 degrees. In order to compensate for the existence of edge restraint within the test slabs, Graddy et al. (2002) reduced the angle θ to 38 degrees for predictions. It was reported that for all deck slabs tested, the predicted punching shear capacities more closely matched those observed than those predicted by the AASHTO and ACI equations.

El-Gamal et al. (2005) proposed a model to predict the punching shear capacity of concrete deck slabs reinforced with FRP or steel reinforcement. The following equation is a modification of the ACI punching shear capacity equation to take into account the amount of restraint provided by the testing system:

$$V_c = 0.33\sqrt{f'_c}\, b_o d \alpha (1.2)^N \text{ (SI units)}$$

Equation 5

where b_o is the critical perimeter at a distance $d/2$ away from the loaded area, N represents the continuity effect of the slab on the punching capacity;

N = 0 (for one span slab in both directions);

N = 1 (for slab continuous along one direction);

N = 2 (for slabs continuous along their two directions);

and (α) is a function of the flexural stiffness of the main bottom reinforcement, the area of the applied load, and the effective depth of the slab:

$$\alpha = 0.62(\rho_f E_f)^{1/3}\left(1 + \frac{8d}{b_o}\right) \text{(SI units)}$$

Equation 6

where ρ_f and E_f are the reinforcement ratio and modulus of elasticity of the main bottom reinforcement, respectively.

The El-Gamal et al. (2005) punching shear capacity model was verified using test data obtained from steel reinforced concrete slabs tested by other researchers (Marzouk and Hussein, 1991; Elstner and Hognested, 1960; Kinnunen and Nylander, 1960; Emam, 1995; Hognested et al., 1964). As seen in Figure 5, the proposed model punching shear capacity predictions were in good agreement with the test results and more accurate than predictions generated using the ACI equation.

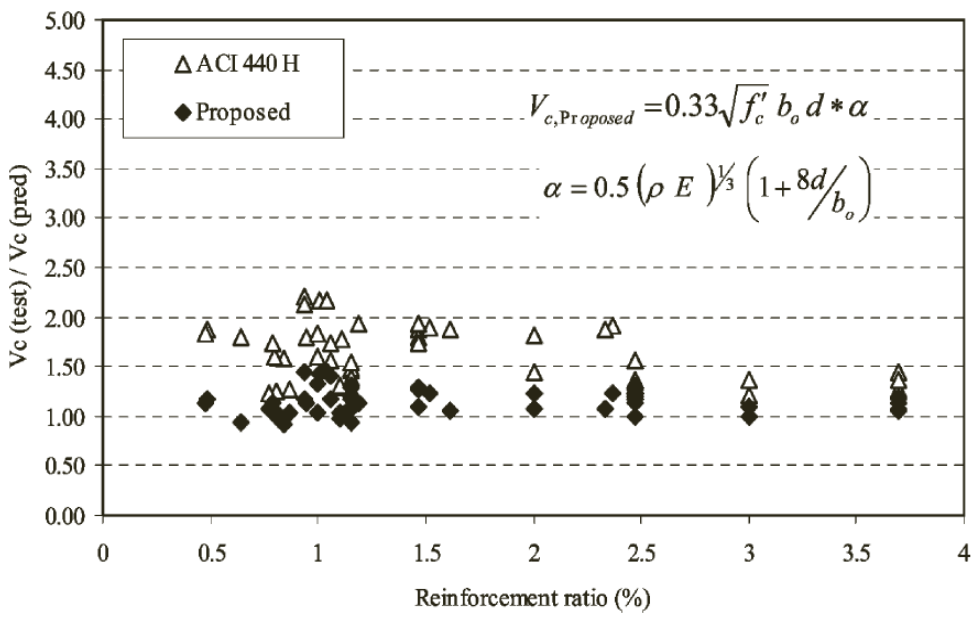

Figure 5: Proposed and ACI Model Punching Shear Capacity Predictions (El-Gamal et al., 2005)

Finite Element Modeling of Reinforced Concrete Using ANSYS

There are many commercial finite element modeling packages available for the analysis of structural systems using solid material models such as: ADINA, ALGOR,

ANSYS, COSMOS, DIANA, LUSAS, NASTRAN, and SIMULA. ANSYS is a commonly used finite element software for modeling reinforced concrete structures. The package provides linear and nonlinear material laws, nonlinear elements, and inelastic material models combined with iterative and direct solvers, allowing for the analysis of reinforced concrete structural assemblies.

Wolanski (2004) studied the flexural behavior of both a conventionally reinforced and a pre-stressed concrete beam using ANSYS (see Figure 6). The conventionally reinforced beam that was modeled was symmetric in geometry and loading about two separate planes, which allowed only one quarter of the beam to be modeled as shown in Figure 6. In order to utilize symmetry within the model, the displacement in the direction perpendicular to both planes of symmetry was set to zero.

The Finite Element Analysis (FEA) for the concrete beams included: non-linear concrete properties, concrete cracking parameters, bilinear steel properties, application of pre-stressing forces, and the addition of self-weight. Pre-stressing forces were applied to the pre-stressed beam model by adding initial strains to the pre-stressing steel elements. The initial strains were determined from the effective pre-stress and the modulus of elasticity of the pre-stressing steel. The analysis of the conventionally reinforced beam model was set up to examine the initial cracking of the beam, yielding of the steel reinforcement, and the strength limit state of the beam. The load-deflection curve generated from the finite element model compared well to the experimental data obtained from Buckhouse (1997) as shown in Figure 7.

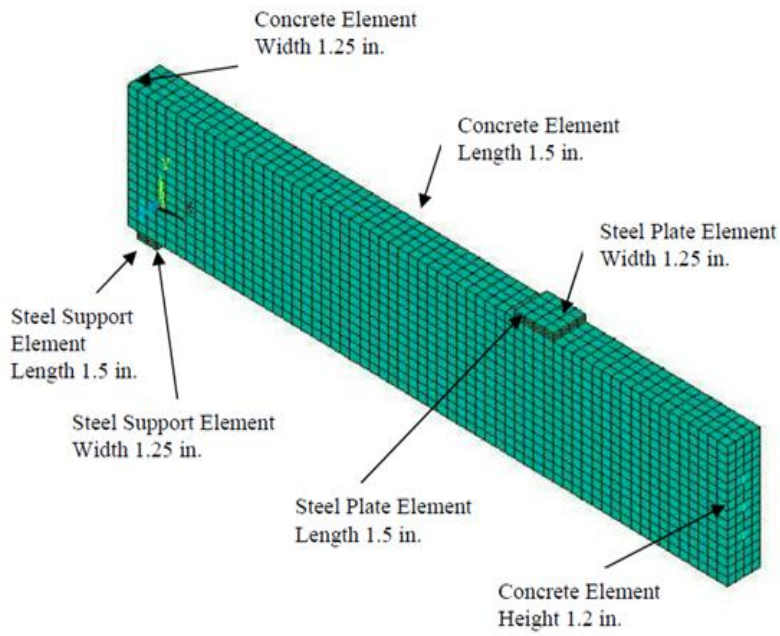

(a)

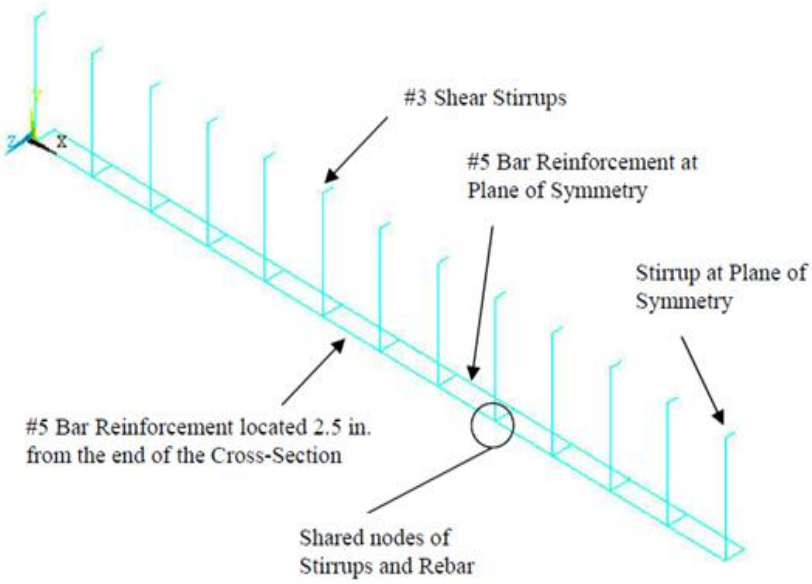

(b)

Figure 6: (a) Mesh of the Concrete, Steel Plate, Steel Support and (b) Reinforcement Configuration for a Quarter of the Beam (Wolanski, 2004)

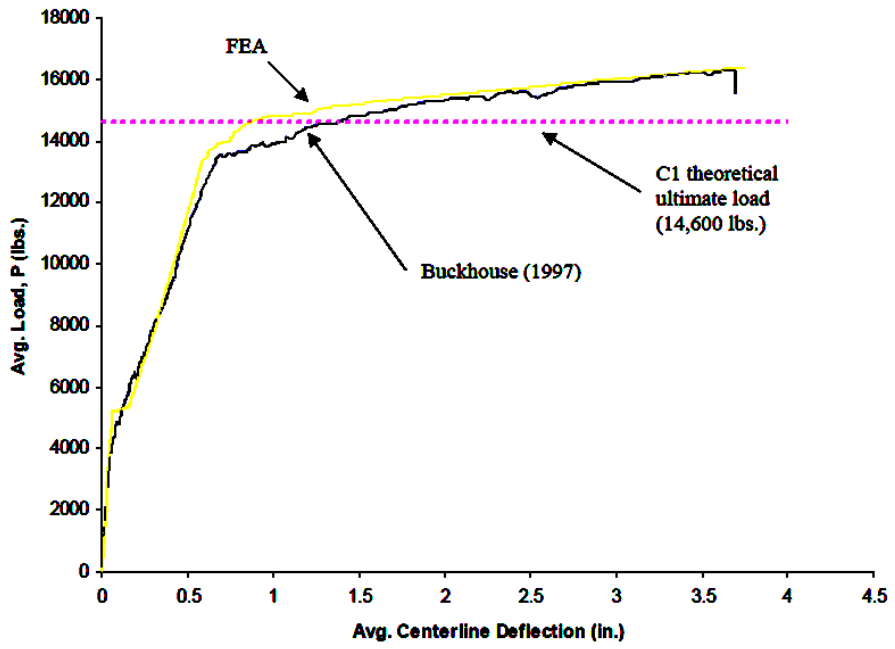

Figure 7: Load versus Deflection Plot (Wolanski, 2004)

Kachlakev et al. (2001) used ANSYS to simulate the linear and non-linear response of concrete beams reinforced with fiber reinforced polymer (FRP) composites. This study stressed the importance of properly selecting the mesh density within the FEM. Multiple convergence studies were performed in order to determine an appropriate mesh density for the reinforced concrete beam model. Three response parameters of interest were examined: mid-span deflection, compressive stress in the concrete at the mid-span, and tensile stress in the steel reinforcement at the mid-span. Convergence was considered to be acquired once the parameter of interest versus mesh density plots seen in Figure 8 “flattened out”; indicating that an increase in the number of elements within the model had a negligible effect on the results.

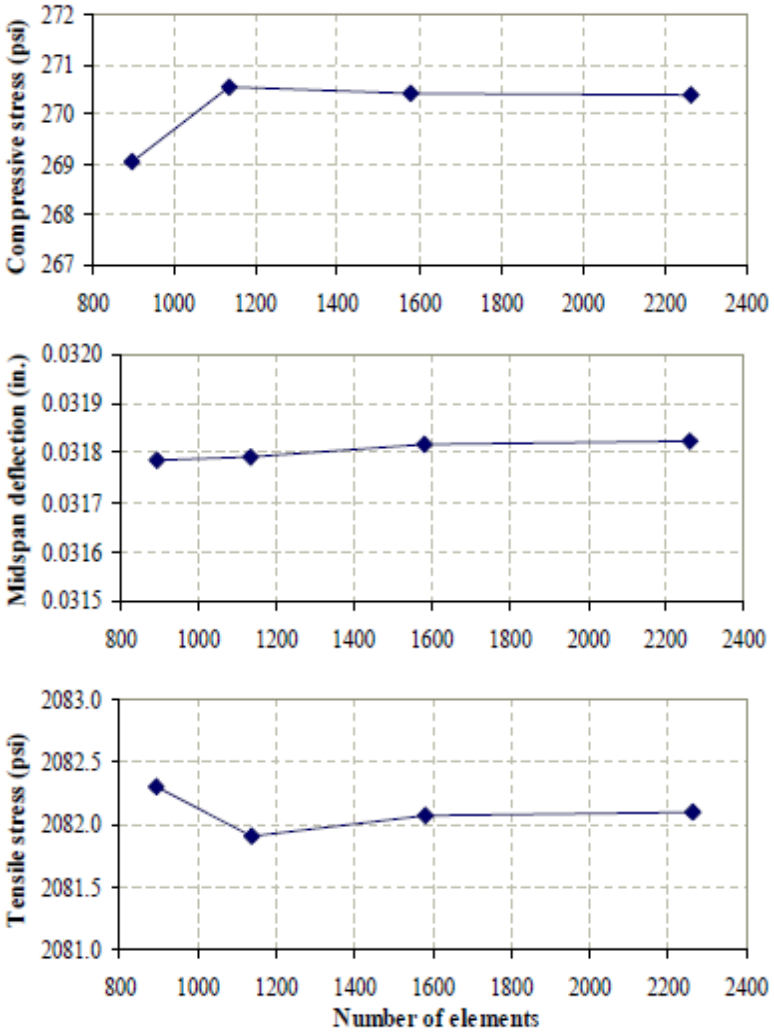

Figure 8: Parameter of Interest versus Mesh Density Plots (Kachlakev et al., 2001)

ANSYS FE Model (SOLID65)

In ANSYS, a solid element called Solid65 is used to model reinforced concrete. The Solid65 element has eight nodes with three degrees of freedom at each node: translations in the nodal x, y, and z directions. The geometry and node locations of the Solid65 element are shown in Figure 9. The element is capable of plastic deformation,

cracking in tension in three orthogonal directions and crushing in compression. The element is also capable of being modeled with or without reinforcement (ANSYS, 2008).

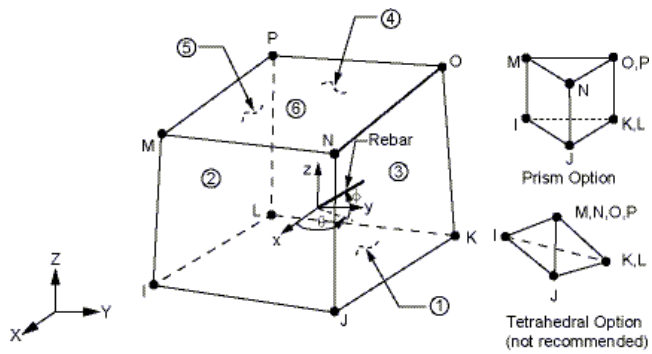

Figure 9: Solid65 – Reinforced Concrete 3-D Solid Element (ANSYS, 2008)

Wolanski (2004) input both linear and multi-linear isotropic material properties in the Solid65 elements to model reinforced concrete's behavior. The linear isotropic material properties included the elastic modulus (E_c) and Poisson's ratio (v) of the concrete. The multi-linear isotropic material properties were input as points from a compressive uni-axial stress versus strain diagram for concrete produced by Kachlakev et al. (2001). The five points of interest are shown in Figure 10. Point 1 was defined as the 30 percent of the ultimate compressive strength (f'_c) point where the corresponding strain was calculated using Hooke's Law. Points 2, 3, and 4 were calculated from the following stress-strain relationship for concrete developed by Desayi and Krishnan (1964):

$$f = \frac{E_c \varepsilon}{1 + \left(\frac{\varepsilon}{\varepsilon_o}\right)^2}$$

Equation 7

$$\varepsilon_o = \frac{2f'_c}{E_c}$$

Equation 8

where, f is the stress at any strain ε (in psi), and ε_0 is the strain at the ultimate compressive strength f'_c. Point 5 in Figure 10 was defined as the ultimate compressive strength which corresponds to a crushing strain for unconfined concrete (ε_0) of 0.003 in/in.

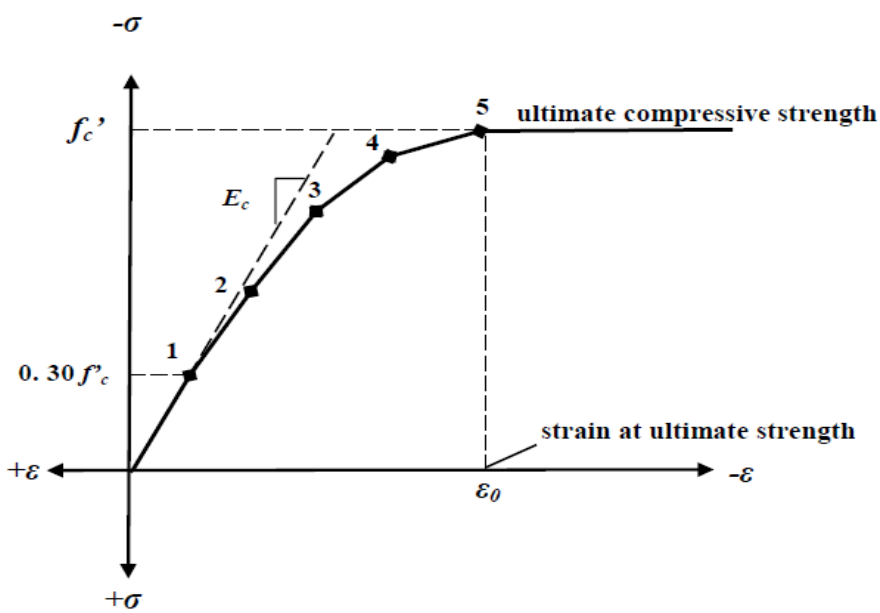

Figure 10: Compressive Uni-axial Stress versus Strain Diagram for Concrete (Kachlakev et al., 2001)

The Solid65 element requires the input of eight parameters to account for cracking and crushing failure modes of reinforced concrete (ANSYS, 2008). Three of the eight parameters are a shear transfer coefficient for an open crack, a shear transfer coefficient for a closed crack, and a stiffness multiplier for a cracked tensile condition. Shear transfer coefficients are used to consider the retention of shear stiffness in cracked concrete. These coefficients range from 0.0 to 1.0, with 0.0 representing a smooth crack

(complete loss of shear transfer) and 1.0 representing a rough crack (no loss of shear transfer). Wolanski (2004) used a coefficient of 0.3 for an open crack, and 1.0 for a closed crack with no convergence problems. The stiffness multiplier is used across a cracked face or for a crushed element and adds a small amount of stiffness to the element to help accelerate convergence of the calculations (ANSYS, 2008).

Willam and Warnke (1975) developed a criterion for failure of concrete due to a multi-axial stress state. The criterion is expressed as follows:

$$\frac{F}{f'_c} - S \geq 0$$

Equation 9

where F is a function of the principal stress state, and S is the failure surface expressed in terms of the remaining five ANSYS cracking/crushing parameters. These parameters consist of: the ultimate uni-axial tensile strength or modulus of rupture (f_r), the ultimate uni-axial compressive strength (f'_c), the ultimate biaxial compressive strength (f'_{cb}), the ultimate compressive strength for a state of biaxial compression superimposed on the ambient hydrostatic stress state (f_1), and the ultimate compressive strength for a state of uni-axial compression superimposed on the ambient hydrostatic stress state of concrete (f_2). The ambient hydrostatic stress state (σ_h) is defined as:

$$\sigma_h = \frac{1}{3}\left(\sigma_{xp} + \sigma_{yp} + \sigma_{zp}\right)$$

Equation 10

where σ_{xp}, σ_{yp}, and σ_{zp} are the principal stresses in the principal directions (ANSYS, 2008). If f'_{cb}, f_1, and f_2, are not input into the model, ANSYS defaults to the following equations based on work done by Willam and Warnke (1975):

$$f'_{cb} = 1.2 f'_c$$

Equation 11

$$f_1 = 1.45 f'_c$$

Equation 12

$$f_2 = 1.725 f'_c$$

Equation 13

However, these stress states are only valid for stress states satisfying the following condition:

$$|\sigma_h| \leq \sqrt{3} f'_c$$

Equation 14

Cracking occurs within a Solid65 element when the principal tensile stress in any direction lies outside the failure surface. When an element cracks, the elastic modulus of the element is set to zero in the direction parallel to the principal tensile stress direction. When all of the principal stresses within the element are compressive and lie outside the failure surface, crushing of the element occurs. Crushing will cause the elastic modulus of the element to be set to zero in all directions, and the element will in effect disappear (ANSYS, 2008). In work done by both Wolanski (2004) and Kachlakev et al. (2001), the crushing capability of the Solid65 element was turned off to avoid convergence problems.

ANSYS uses a three-dimensional failure surface for concrete depicted in Figure 11 for states of stress that are biaxial or nearly biaxial. The important nonzero principal stresses are in the x and y directions, which are represented by σ_{xp} and σ_{yp}, respectively. The three surfaces shown are for σ_{zp} slightly greater than zero, σ_{zp} equal to zero, and σ_{zp} slightly less than zero. The three failure surfaces are shown as projections on the σ_{xp} - σ_{yp} plane, and the mode of material failure is a function of the sign of σ_{zp}. For example, if σ_{xp} and σ_{yp} are both negative (compressive) and σ_{zp} is slightly positive (tensile), cracking would be predicted in a direction perpendicular to σ_{zp}. However, if σ_{zp} is zero or slightly negative, the material is assumed to crush (ANSYS, 2008).

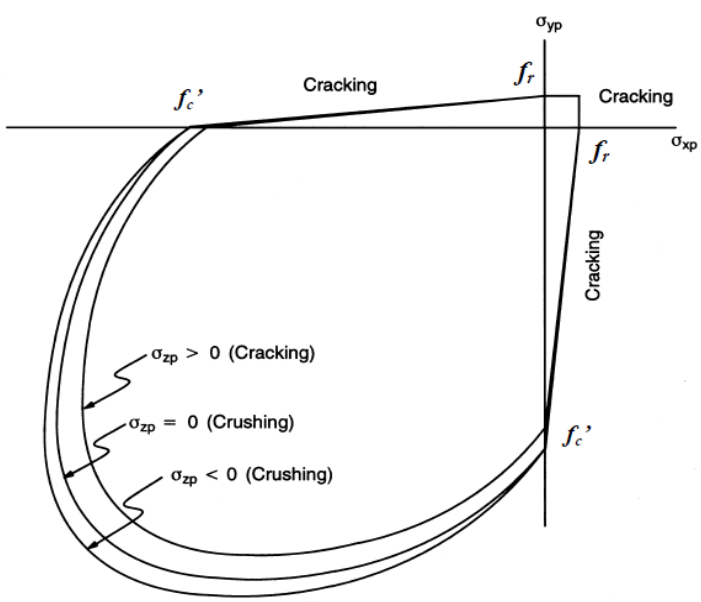

Figure 11: Three-Dimensional Failure Surface for Concrete (ANSYS, 2008)

ANSYS FE Modeling of Reinforcement

Unique to reinforced concrete over plain concrete is the choice of how to model the composite nature of the material. Tavarez (2001) explains both the smeared and discrete methods to model the reinforcement in a three-dimensional reinforced concrete FEM. The appropriate technique is dependent on the function of the structural model and the level of detail required in the results.

In the smeared model shown in Figure 12a, the reinforcement is assumed to be uniformly distributed within user defined concrete elements. The material properties of these defined elements are based on the composite action of the individual properties of concrete and reinforcement. In ANSYS, up to three reinforcement materials can be added to the concrete in a Solid65 element. The reinforcement is assumed to have uni-axial stiffness only and is smeared throughout the element. Rebar specifications include material properties, volume ratio of rebar to concrete, and the orientation angles of the rebar (ANSYS, 2008). Tavarez (2001) states that the smeared model is usually applied for large structural models where reinforcement details are not essential to capture the overall response of the structure.

In the discrete model shown in Figure 12b, the reinforcement is modeled using bar or beam elements. The concrete and the reinforcement mesh share nodes so that the concrete occupies the same regions that are occupied by the reinforcement. The drawback of the discrete model is the restriction of the concrete mesh by the location of the reinforcement and the inability to subtract the volume of the reinforcement from the concrete model.

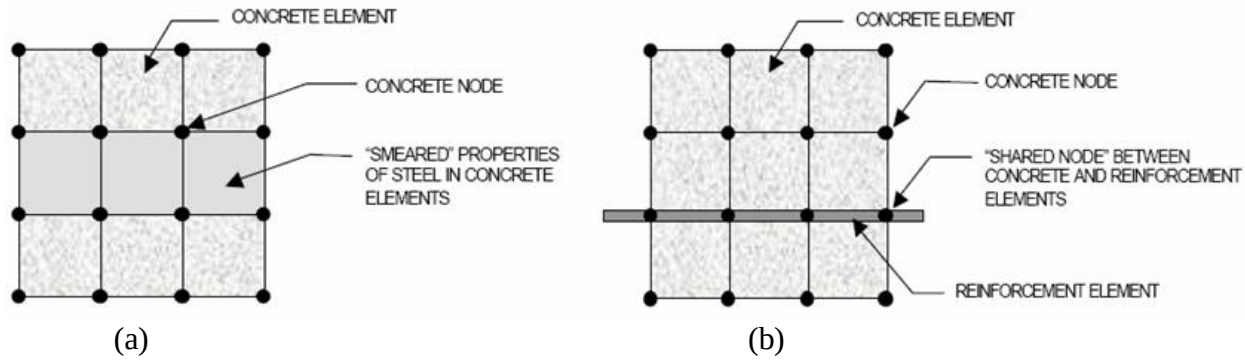

Figure 12: (a) Smeared and (b) Discrete Models of the Reinforcement in Reinforced Concrete (Tavarez, 2001)

In work done by both Wolanski (2004) and Kachlakev et al. (2001), Link8 elements were used to discretely model the reinforcement instead of adding rebar specifications to the Solid65 elements. The Link8 element is a 3-D spar element that has two nodes with three degrees of freedom: translations in the nodal x, y, and z directions (ANSYS, 2008). The element is capable of plastic deformation. The geometry and node locations for the Link8 element type are shown in Figure 13.

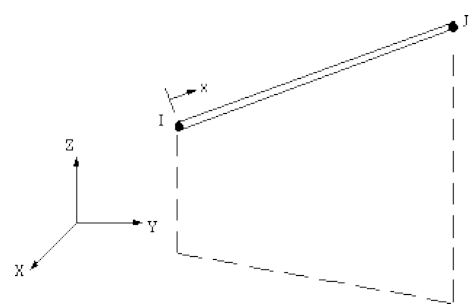

Figure 13: Link8 –Three-Dimensional Spar Element (ANSYS, 2008)

Wolanski (2004) input both linear and bilinear isotropic material properties in the Link8 elements to model the reinforcement's behavior. The isotropic material properties

included the modulus of elasticity (E) and Poisson's ratio (v) of the reinforcement. The bilinear isotropic material properties included the yield stress (f_y) and the hardening modulus of the reinforcement. Each of the Link8 elements were modeled through the concrete nodes that were created when the concrete volume was meshed. As a result, no separate mesh of the reinforcement was needed.

ANSYS Linear and Nonlinear Analysis

In ANSYS, the reinforced concrete material model predicts either elastic behavior, or cracking / crushing behavior. If elastic behavior is predicted, the concrete is treated as a linear elastic material, and if cracking or crushing behavior is predicted, the material is treated as a nonlinear material (ANSYS, 2008).

The linear behavior of the Solid65 element is defined by a stress-strain matrix that is based on the number of reinforcing materials, the ratio of volume of reinforcing material to total volume of element, a stress-strain matrix for concrete, and a stress-strain matrix for reinforcement (ANSYS, 2008). The stress-strain matrix for concrete is derived by specializing and inverting the orthotropic stress-strain relations defined by a compliance matrix to the case of an isotropic material with an elastic modulus (E_c) and Poisson's ratio (v) of concrete. The stress-strain matrix for reinforcement is dependent on the orientation of the reinforcement within the element and Young's modulus of the reinforcement (E).

The nonlinear behavior of the Solid65 element considers both concrete and reinforcement behavior. The elastic stress-strain matrices for the concrete and the reinforcement are adjusted for each failure mode. When a nonlinear analysis is

performed, the total applied load to the finite element model is divided into a set of load increments or load steps. The stiffness matrix of the reinforced concrete model is adjusted upon the solution of each load step to replicate nonlinear changes in structural stiffness before moving on to the next load step (ANSYS, 2008). ANSYS defaults to using the Newton-Raphson approach to adjust the model's stiffness. By this approach, convergence is attained at the end of each load step within specific tolerance limits. Newton-Raphson equilibrium iterations for a single degree of freedom nonlinear analysis are shown in Figure 14.

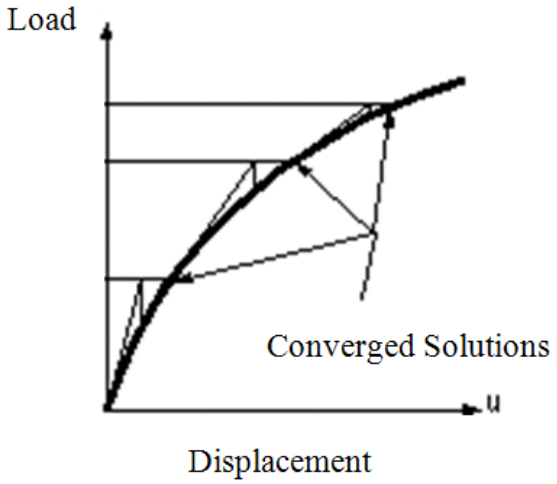

Figure 14: Newton-Raphson Iterative Solution (3 load increments) (ANSYS, 2008)

The Newton-Raphson approach calculates an out-of-balance load vector prior to each solution. This vector is defined as the difference between the restoring forces (the loads corresponding to the element stresses) and the applied loads. A linear solution is then performed, using the out-of-balance loads, and checks for convergence. When the

convergence criteria are not satisfied, the out-of-balance load vector is reevaluated, the model's stiffness matrix is updated, and a new solution is obtained (ANSYS, 2008).

The Newton-Raphson approach was used in the non-linear analysis performed by both Wolanski (2004) and Kachlakev et al. (2001). Transverse loads were applied incrementally as required by the Newton-Raphson procedure, ranging in magnitude from zero to a load corresponding to failure. The size of the load increment varied along the load-deformation curve. Load increments were smaller in areas where convergence was difficult to obtain which typically corresponded to areas of behavioral interest such as concrete cracking and steel yielding.

Wolanski (2004) utilized a static analysis type with the assumption of small displacements. The convergence criteria for the analysis included force and displacement, which were left at the ANSYS default values up until cracking initiated. It was reported that at loads beyond the onset of cracking, convergence was unobtainable using the default values. Therefore, the tolerances for force and displacement were set to five times the default values when capturing behavior beyond initial cracking. The convergence criteria used was considered to be adequate in capturing the correct response of the beams.

CHAPTER 3 - RESEARCH METHODOLOGY

Introduction

This chapter presents an overview of the research methods used in the laboratory investigation and the finite element analysis. The laboratory work consisted of designing a reaction frame to hold a sample test specimen and then monotonically loading a specimen mounted in the frame to failure in order to validate the effectiveness of the support frame in replicating field conditions. The results of this test were also used to better predict the behavior of the test specimens to be used in future rolling wheel load tests. The finite element analysis included modeling of the deck panel in ANSYS and observing its response as it was analytically loaded to failure. The results of this analysis were used in conjunction with the test data in evaluating the ability of the test frame to provide the desired edge restraint to the deck specimens. ANSYS modeling was also used in the design of the test support frame, itself.

Description of Test Specimen

Stordahl (2009) investigated candidate configurations of full-scale bridge deck specimens to be used for both static and fatigue laboratory testing for the basic Caltrans study. The test specimen configurations that were investigated replicated a section of the deck of a typical Caltrans box girder bridge. Stordahl (2009) used Visual Analysis, a commercial finite element program for structural engineering analysis and design, in his investigation. Using multiple plate models, Stordahl (2009) identified a deck specimen

for laboratory testing that captured realistic transverse bridge deck stresses when loaded with a truck tire footprint in the center and at various locations along its length.

This bridge deck specimen was 7 feet wide by 8.5 feet long by 6.5 inches thick. The thickness of the deck slab was chosen to be consistent with Caltrans standard details. The width of the slab was selected to insure that when loaded by a wheel, the affected area in the center of the slab would have similar behavior in the transverse direction to a continuous bridge deck. The length was chosen so that when a wheel load traveled in the center of the slab in the longitudinal direction, there would be a significant portion of slab whose behavior would not be affected by the leading and trailing edges.

The modeling work done by Stordahl (2009) used linear elastic analysis. The boundary conditions imposed on the test model included fully clamped conditions along the longitudinal edges and simply supported conditions along the transverse edges of the slab. An analytical model of the full bridge was built to validate that transverse stresses in the proposed test panel matched those in a full bridge. The full bridge model was simply supported and spanned 80 feet in the longitudinal direction. In both of the models, the applied load used was based on a practical load carrying capacity of a dual tire of 15,000 pounds and was uniformly distributed over a contact area that simulated the footprint of a standard truck wheel load.

As seen in Figure 15, the transverse stress profiles in the top of the deck for the test model and the full bridge model matched well. This indicated that the clamped plate model was able to replicate realistic transverse bridge stresses. It was also discovered that when the wheel load passed along the test slab in the longitudinal direction, an

interior length of the slab existed in which the transverse stresses were relatively unaffected by the lead and trailing discontinuous transverse edges. The extent of this interior section, which is approximately 3.5 feet in length, is delineated in Figure 16 as the zone of relatively constant transverse stress response.

The full-scale bridge deck specimen that was tested in this investigation was of the same configuration as the proposed slab to be used in future testing. Following the work of Stordahl (2009), the deck specimen selected for testing, shown in Figure 17, was a slab 8 feet 5 ½ inches long by 7 feet wide by 6.5 inches thick, reinforced with two mats of steel. The reinforcement layout in the specimen was taken directly from standard design details provided by Caltrans for their box girder bridges. Reinforcement consisted of number four and number five bars in straight, bent, and truss bar configurations (see Figure 17). Detailed drawings of the slab specimen are provided in Appendix A. This was the deck panel configuration subsequently used in the monotonic test to failure conducted in this investigation.

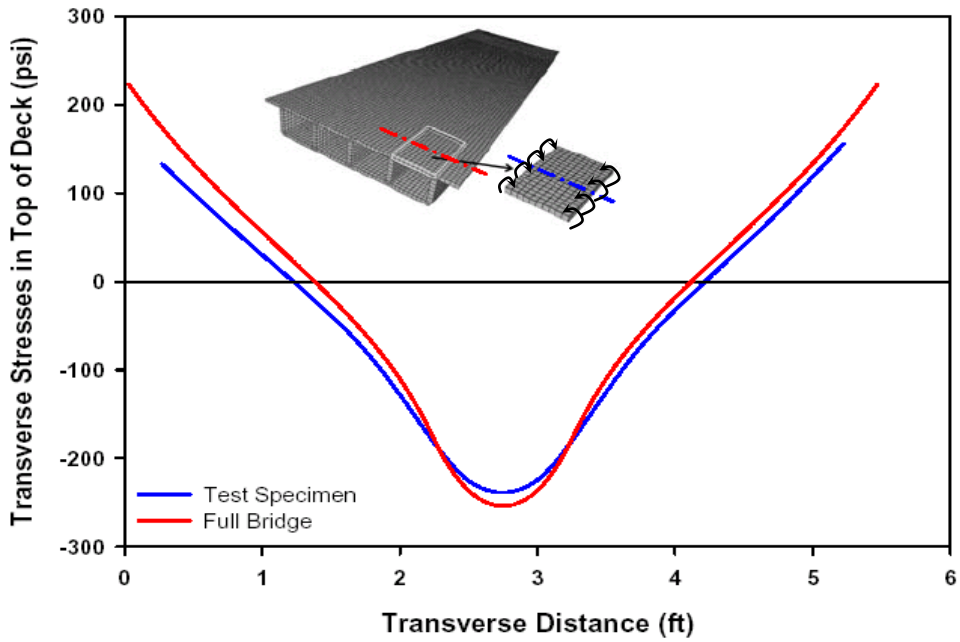

Figure 15: Transverse Stresses in the Top of the Deck for the Test Model and the Full Bridge Model (Stordahl, 2009)

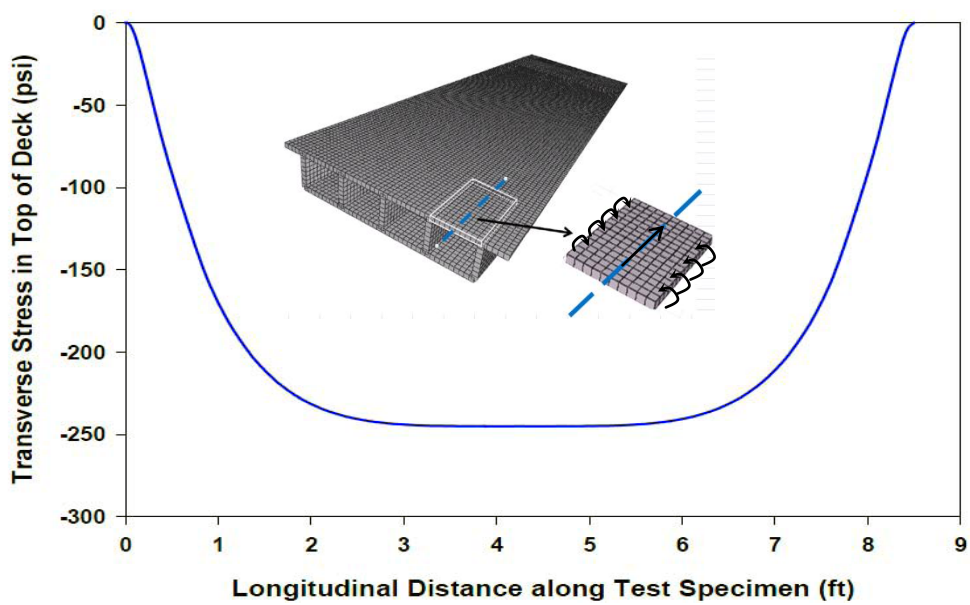

Figure 16: Transverse Stresses in the Top of the Deck Under the Wheel Load as it Moves Along the Test Model (Stordahl, 2009)

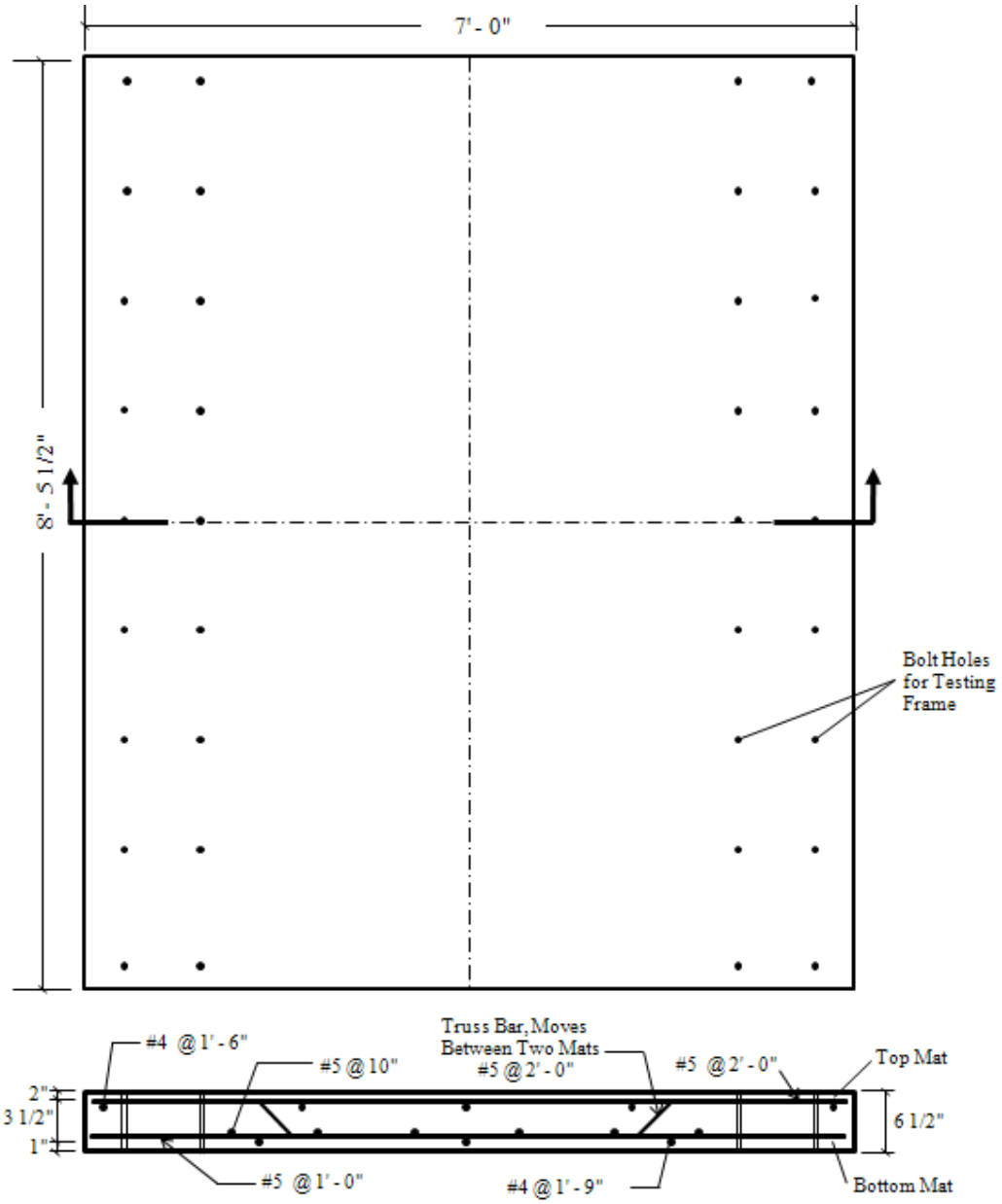

Figure 17: Dimensions and Reinforcement Details of Test Specimen

Laboratory Testing Frame

Early work on this project was devoted to designing a testing frame to support the deck test panels described in the previous section for the purpose of fatigue testing. The support frame was designed with the primary intention of providing full restraint (no rotation or vertical translation) along the longitudinal edges of the deck specimens when trafficked by a rolling wheel load of up to 30 kips in magnitude. The frame was also designed to provide simple support of the leading and trailing edges of each deck panel to ensure that mid-span transverse stresses and distresses are minimally affected by these discontinuous edges when a moving wheel load passes along the full length of the test slab. Another important design consideration was to provide access to the underside of the test specimens for the purposes of monitoring crack development and measuring displacements.

The design procedure consisted of running various solid models of the candidate support frame and mounted deck panels within ANSYS, and using an iterative process until a support frame configuration was developed that satisfied the criteria described above, while still maintaining an economical design. This section first discusses the support frame design that was chosen, followed by an overview of the ANSYS modeling work that was done to arrive at the final design.

The testing frame configuration that was selected for this study was similar to the support frame used by El-Gamal et al. (2005) (Figure 2). Limited information was available on the manner in which that frame was designed, or to what extent it successfully generated the desired support conditions.

Description and Design of Support Frame

As can be seen in Figure 18, the proposed support frame was designed to simultaneously test four deck panels and consists of two continuous support beams along the longitudinal edges of the panels with short cross beams under the transverse edges that are shared between adjacent panels. Access holes are located in the longitudinal beams under each test panel to facilitate their installation and subsequent response monitoring during testing. Rotation and translation restraint is provided along the longitudinal edges of the panel by a clamping mechanism detailed in Figure 19, in which the test panel is sandwiched between the support beam and a 10 inch top channel using a double row of ½ inch diameter bolts. The bolts are spaced 12 inches on center in the longitudinal direction and 7 inches on center in the transverse direction. Candidate sizes for the top channel as well as the bolt sizes and spacing's were based on the testing frame used by El-Gamal et al. (2005). Conservative hand calculations were performed to ensure bolt tensile capacities would not be exceeded during testing.

For the main longitudinal support members of the test frame, consideration was given to using W and HSS sections. W sections were perceived to offer simplicity in implementing the bolted panel restraint system but offer poor torsional resistance in the transverse direction of the panels. HSS sections were thought to offer better torsional resistance to the applied load but involved challenges in implementing the bolt restraint system. Therefore, it was decided to use W sections with full depth web stiffeners. The depth of the wide flange beams was driven by the physical height required for access to the underside of the test specimens, which, after constructing a full size mockup of the frame and panels, was set at 24 inches. Note that this mockup was also used to evaluate

various access hole configurations and sizes for reasonable egress and exit, resulting in these holes being nearly full depth of the beam section and 20 inches wide. A flange width of approximately 12 inches was chosen to allow the bolts that clamp the edge of the panels to comfortably straddle the beam web. The remaining design variables (i.e., specific beam size, web stiffener size and spacing, etc.) were left to the ANSYS modeling work, which is discussed in the next section. For the full drawings and specifications of the support frame that was manufactured see Appendix A.

ANSYS Modeling

All of the test frame models that were analyzed in ANSYS consisted of two steel top channels, a concrete slab with dimensions matching those of the test specimen, and steel support beams. Variables in the analyses included: beam size, stiffener size, stiffener spacing, location of access holes, and size of access holes. The concrete was modeled with the Solid65 element, which was previously introduced in Chapter 2. All of the steel in the frame was modeled with the Solid45 element, which is similar to the Solid65 element in that it has eight nodes with three translational degrees of freedom at each node. The concrete and steel were modeled as volumes with mesh sizes that varied for each model configuration created. Each model assumed full contact at all steel-concrete interfaces. Further, a model was also built in ANSYS of the concrete test specimen with its longitudinal edges fully restrained to provide a means to compare the ideal behavior of the test specimen with the results obtained for a test specimen clamped in the various test frame models.

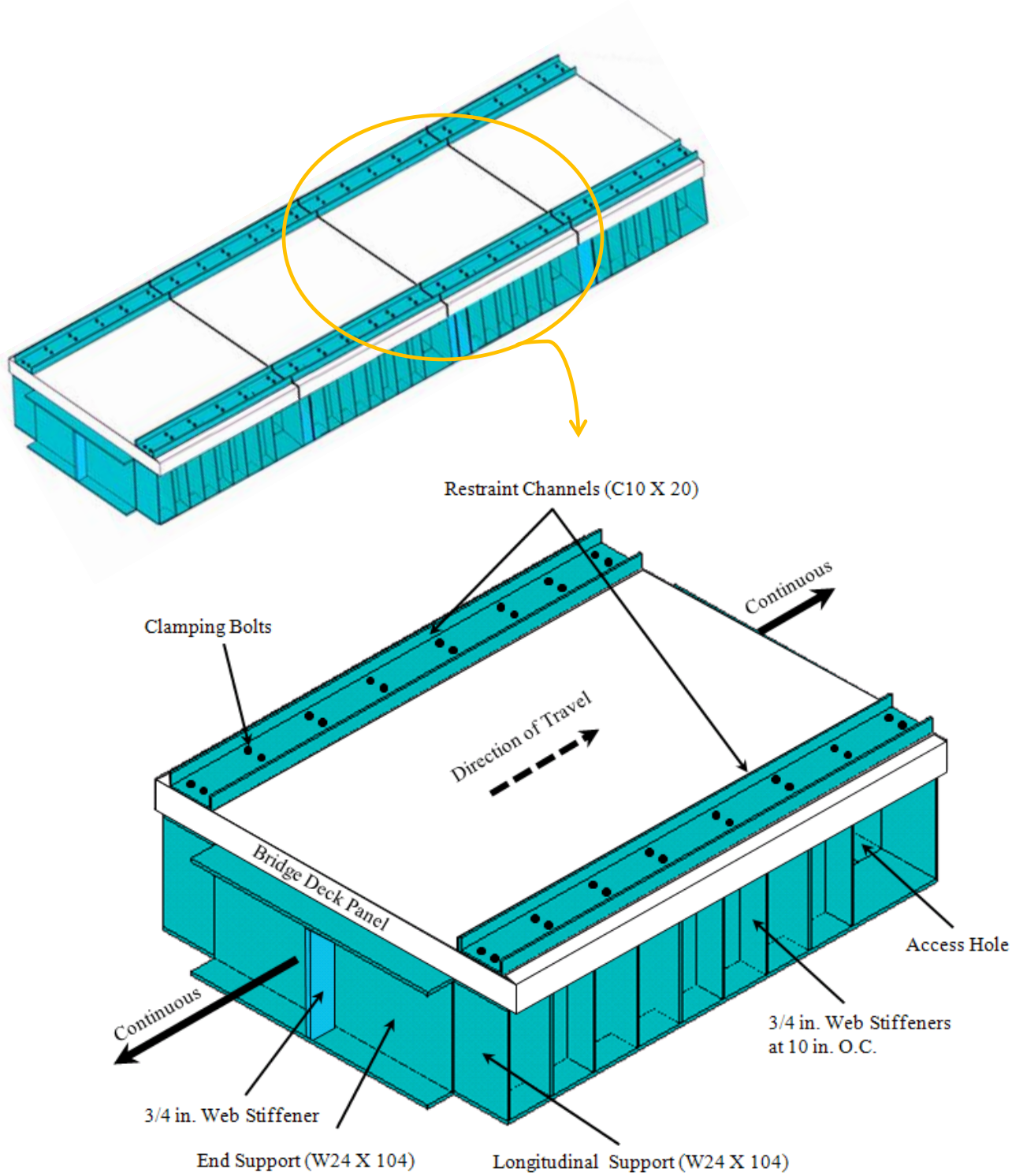

Figure 18: Three-Dimensional Geometry of Testing Frame for a Single Deck Specimen

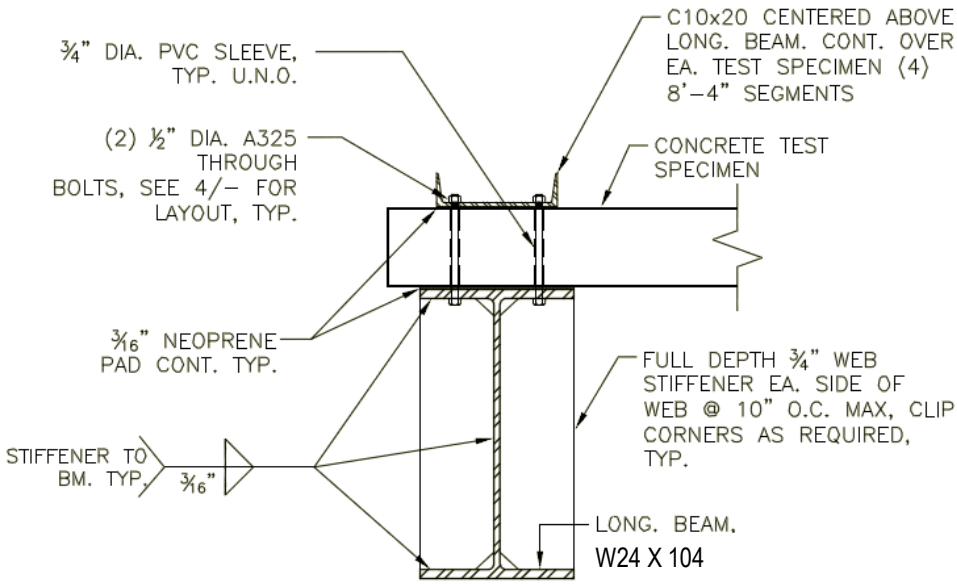

Figure 19: Clamping Detail for Test Specimen

The modeling work done for the design of the testing frame was based on linear elastic analysis at the expected load levels to be used in the rolling wheel load tests. The boundary conditions applied to the test frame were pinned conditions on the bottom faces of the support beams (where they are expected to rest on the floor). The boundary conditions imposed on the fully restrained slab model were the same as those used in the modeling work done by Stordahl (2009), which consisted of fixed-fixed conditions along the longitudinal edges and simply supported conditions along the transverse edges of the slab. In all of the models, the applied load used was based on a practical load carrying capacity of a dual tire of 15,000 pounds and was uniformly distributed over a contact area that simulated the footprint of a standard truck wheel load. It should be noted that the ANSYS modeling procedure is discussed in much greater detail for the non-linear finite element analysis presented later in this chapter.

Test frame models with varying sizes of support beams were analyzed first. It was determined that vertical stiffeners needed to be added to the models in order to obtain the required torsional stiffness of the longitudinal support members. The location and size of the access hole along each section of the longitudinal support members was chosen such that its presence did not significantly affect the stiffness of the member while providing the necessary access to the underside of the test specimens. More sophisticated models were built that incorporated the presence of the pre-tensioned bolts and neoprene pads within the testing frame; however, the difference in results from the less complex models were insignificant.

After numerous test frame models were analyzed, a configuration was chosen such that the transverse behavior at the mid-span of the concrete slab in the longitudinal direction closely matched that of the fully restrained slab model. As seen in Figure 20, the plots of transverse stress profiles in the top of the deck for the fully restrained slab model and the selected test frame model configuration matched well. This indicated that the chosen support frame design would provide the clamped conditions needed to produce the desired distribution of flexural stresses in the test panels. This design consisted of W24x104 longitudinal beams with ¾ inch web stiffeners at 10 inches on center along the beam length.

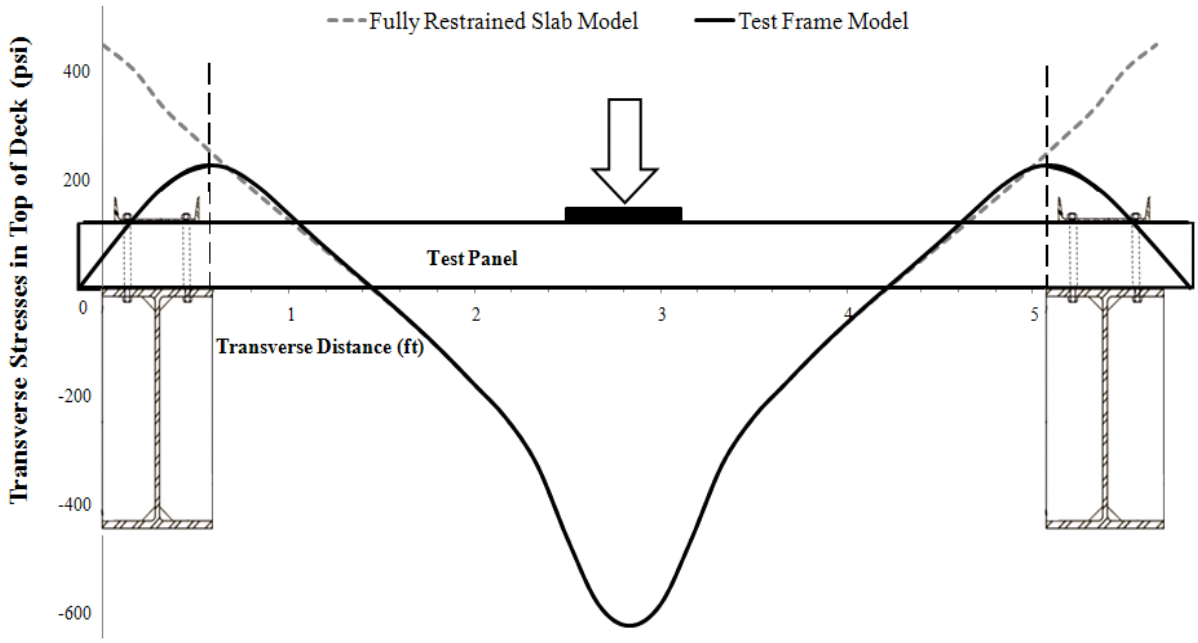

Figure 20: Transverse Stresses in the Top of the Deck for the Fully Restrained Slab and Test Frame Model

Experimental Study

This section discusses the laboratory methodology used to construct and statically load test a full-scale bridge deck panel to failure in the test frame.

Test Specimen Construction

The test specimen was constructed using locally available materials. The slab was reinforced with standard grade 60 rebar, and cast with concrete from a local batch plant using a mix design similar to that used by Caltrans in their bridges. The specified concrete proportions for 1.0 cubic yard of concrete were 1644 pounds coarse aggregate (#4 – ¾”), 1184 pounds fine aggregate, 170 pounds Class F fly ash, and 516 pounds Portland cement (Type I/II) with a water-cement ratio of 0.47 and 3 percent entrained air.

These mix proportions were expected to provide a slump of 4 inches and a 28-day unconfined compression strength of 4,000 psi. It should be noted that the water cement ratio of the as delivered concrete was 0.36, obviously much lower than that specified. In addition, it was discovered that the air entrainment admixture had been omitted from the mixture, and the resulting measured air content at the time of casting was less than 1.5 percent. Both of these errors would account for the higher than desired concrete strength of 7,618 psi at 28 days. The top surface of the deck slab was finished by hand to obtain a flat and smooth surface. The test specimen was then sprayed with a water based pigmented curing compound, followed by a seven-day water cure. Figure 21 shows the deck specimen both before and after the concrete was poured.

Material Testing

Concrete test cylinders 6 inches in diameter by 12 inches long were used to determine the compressive strength and elastic modulus of the concrete on the day the slab was tested. The average compressive strength and elastic modulus of the concrete were 8,040 and 5,053,393 psi respectively. Rectangular beams 6 inches wide by 6 inches deep by 20 inches long were used to determine the modulus of rupture of the concrete. The average rupture modulus on the day the slab was tested was 766 psi. All of the cylinder and rectangular beam specimens were subjected to similar environmental conditions as the test slab.

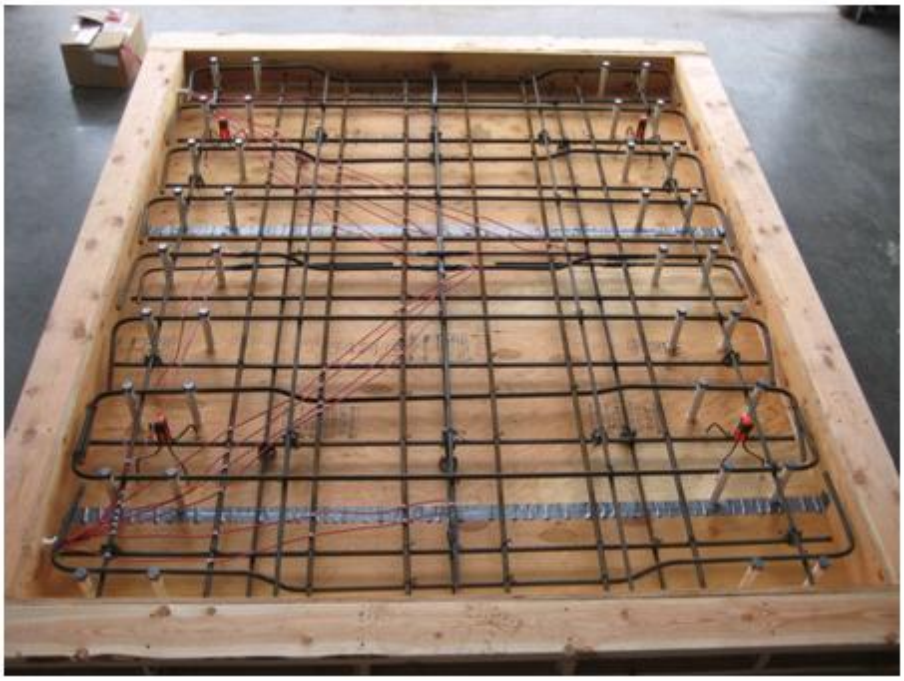

(a)

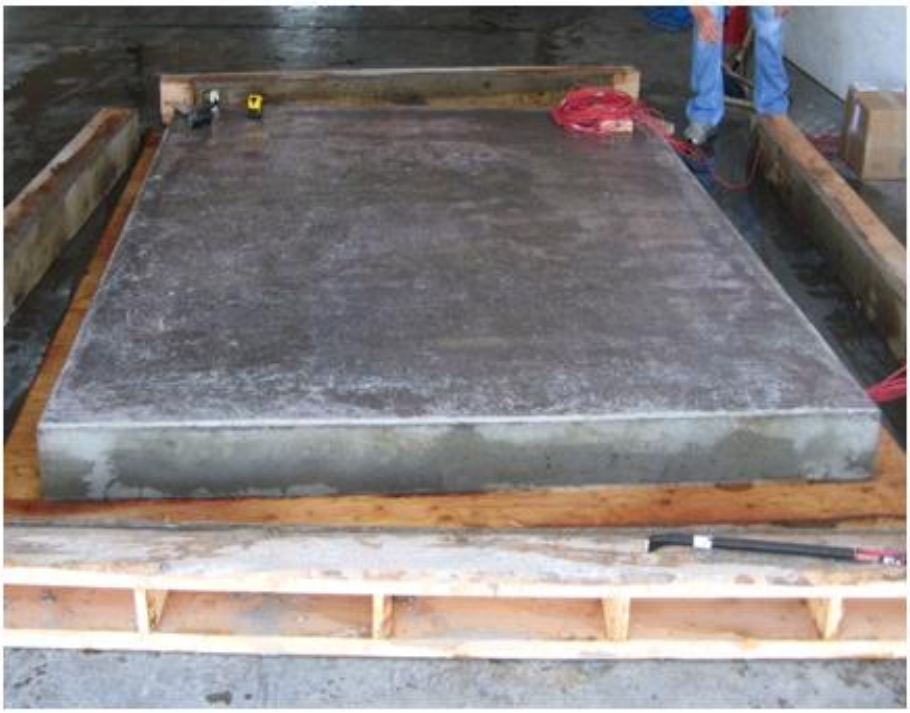

(b)

Figure 21: Test Specimen (a) Before and (b) After Concrete Pour

The mechanical properties of the reinforcing steel were determined by performing tensile tests on representative pieces of rebar set aside for this purpose during construction. The average yield strength and ultimate tensile strength were 64,706 and 106,713 psi respectively. All material sampling and testing was conducted in substantial compliance with ASTM standards.

Test Setup and Loading Procedure

The deck specimen was tested up to failure using a concentrated load acting in the center of the specimen. The load was delivered through a 2.5 inch-thick A-36 steel loading plate with a contact area of 12 x 20 inches. A 3/16 inch thick Low Density Polyethylene (LDPE) bearing pad was used between the steel plate and the concrete surface. The contact area that was used was based on the following relationship for predicting a 11R24.5 truck tire contact area developed by Fernanado et al. (2006):

$$A = 41.9417 + 0.0087T_L - 0.2228T_P$$

Equation 15

where, A is the predicted tire area (in^2), T_L is the tire load (lb.), and T_P is the tire inflation pressure (psi). Assuming a maximum allowed tire load and tire pressure of 10,000 lb. and 150 psi, respectively, yielded a predicted tire area of 96 in^2. Using a tire imprint length to width ratio of 1.2 gave a contact area of 12 inches by 8 inches for a single tire. Incorporating a minimum allowed tire spacing (centerline to centerline) of 12.6 inches for a dual tire truck yielded a total contact area of roughly 12 inches by 20 inches (Figure 22).

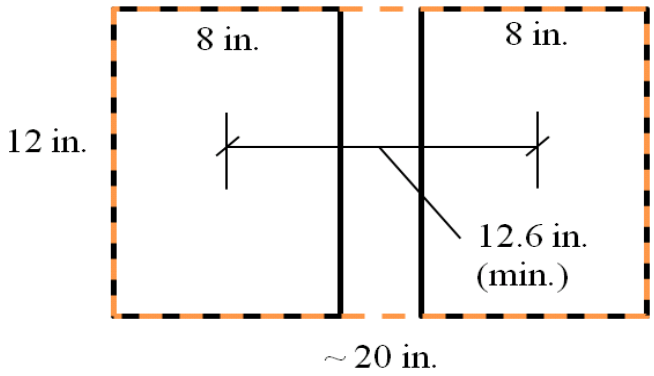

Figure 22: Total Truck Tire Contact Area

The slab support frame was able to accommodate four test specimens placed end-to-end. For this study, the single test specimen was installed in one of the middle two bays of the frame. All of the clamping bolts were tightened to the same level of torque using 12,000 pound tension indicating washers. The minimum bolt pretension force needed for A325 ½ inch bolts is 12,000 pounds (American Institute of Steel Construction, Inc., 2005). LDPE pads, 3/16 inches thick, were used at all interfaces between the steel members and the concrete test specimen.

A loading yoke assembly was constructed to apply the static load to the test specimen. Referring to Figure 23, the overhead yoke consisted of a W16x100 cross beam that supported the hydraulic ram on the center point of the panel and two additional W16x100 beams that supported each end of the cross beam. Each ends of these beams were tied back down to the test frame using four high strength (125 ksi) all-thread rods. The entire assembly was shored vertically and laterally with a simple wood frame to carry its self-weight and any incidental horizontal loads before and after the load was applied to the slab.

As mentioned previously, the support frame was designed with two access holes (one in each longitudinal frame member) in each of the four testing bays. An ANSYS run done specifically on this static test setup revealed that the longitudinal beams were overstressed at the anchorage locations in the area of the access holes. Therefore, these holes were intentionally not cut during frame manufacture. As access was still required to the underside of the test specimen in this test, a hole was cut in one of the transverse supporting members of the test frame (see Figure 23a).

The load was monotonically applied using a 200-kip capacity hydraulic jack controlled by a manually operated pump. The load was stopped at 25-kip intervals throughout the test for crack mapping purposes. A one foot square grid was drawn on the top and bottom surfaces of the slab prior to testing. Cracks were mapped on the entire top surface and on one quarter of the bottom surface of the slab (only one quarter of the bottom surface was readily accessible during the test).

Instrumentation

The instrumentation used was similar to that employed by past researchers including El-Gamal et al. (2005) and El-Ragaby et al. (2007), and included strain gauges, LVDTs, and a load cell. The locations of the strain gauges and LVDTs are schematically presented in Figure 24. Instrumentation was located to obtain vertical deflections along the centerline of the panel in both the transverse and longitudinal directions as well as strains in the transverse and longitudinal reinforcing steel along these same centerlines.

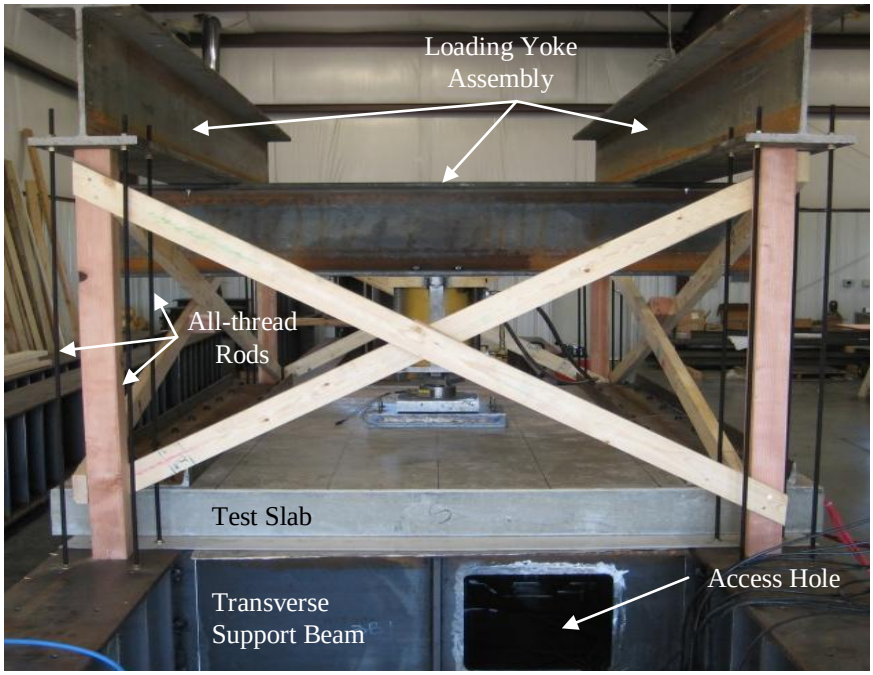

(a)

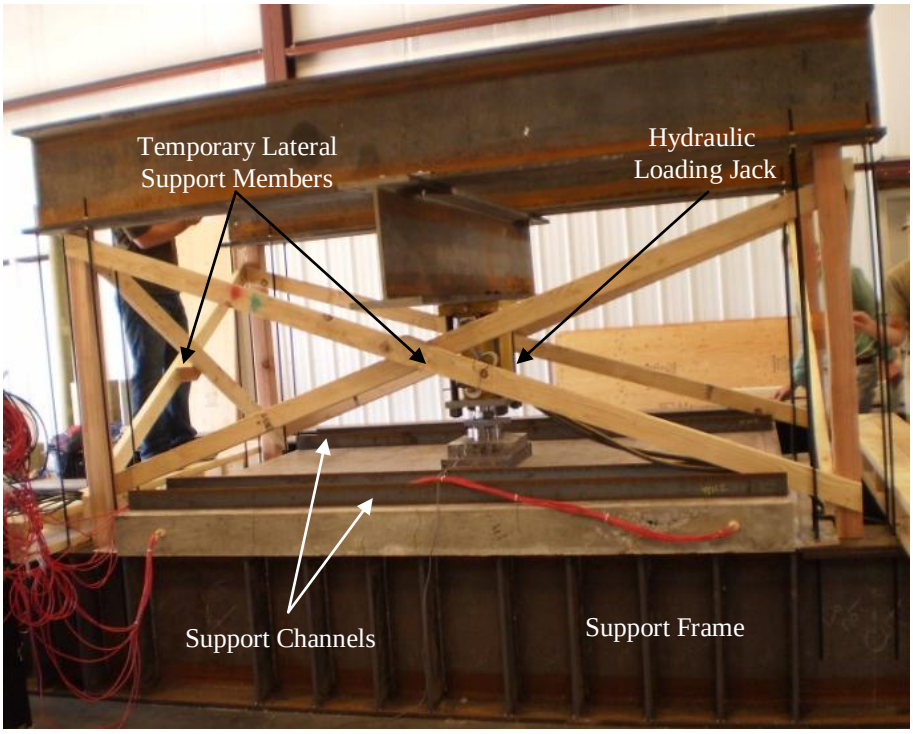

(b)

Figure 23: Photographs of the Test Setup (a) Front View, (b) Side View

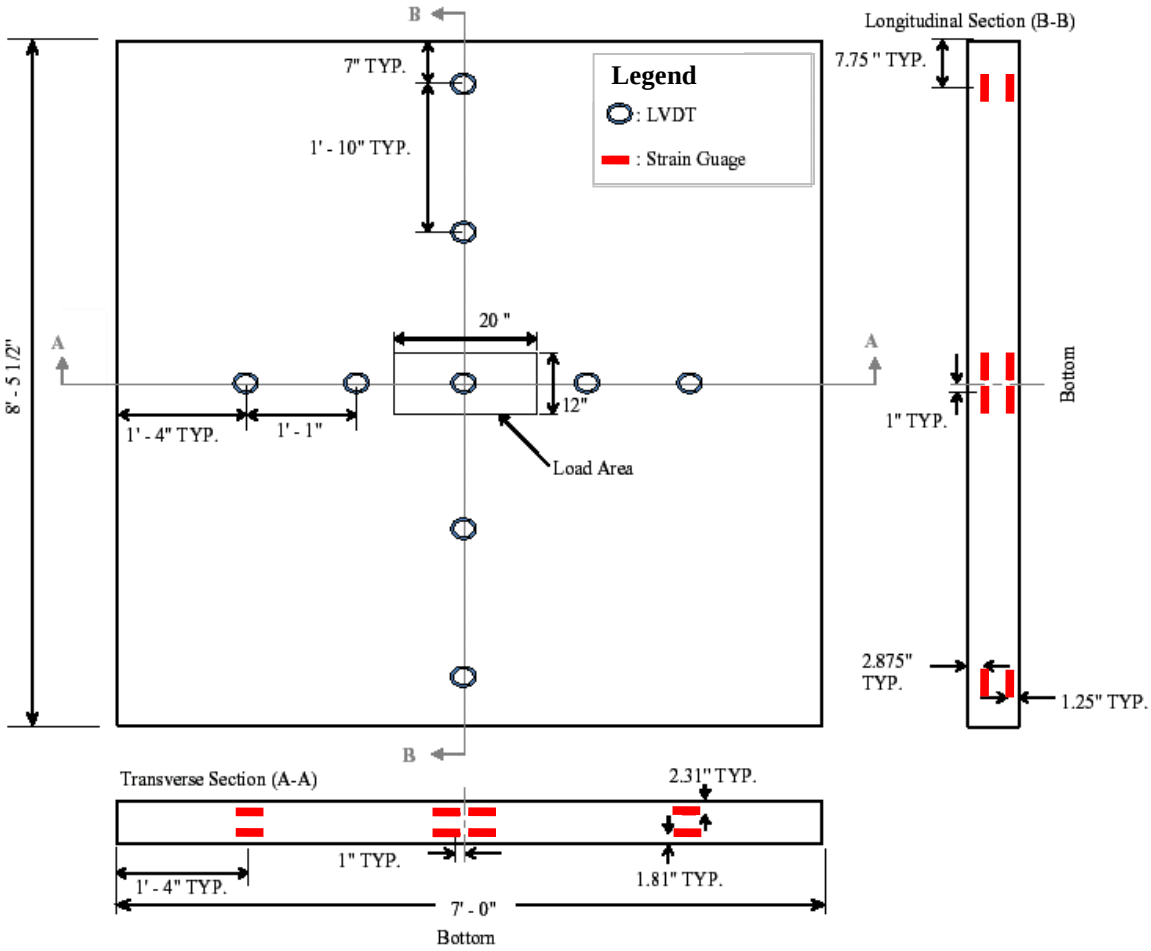

Figure 24: Instrumentation Layout for Test Specimen

Specific reinforcing bars were instrumented with general-purpose resistance foil-backed strain gauges purchased from Micro-Measurements Group, Inc (Raleigh, NC). Each gauge had an active gauge length of 0.125 inches and a resistance in ohms of 350±0.3%. The strain gauges were installed at 16 different locations to measure strains in the top and bottom reinforcing steel in both the transverse and longitudinal slab directions. The strain gauges were bonded to both the top and bottom surface of the steel reinforcement to eliminate the effects of local bending in the bars. The process of bonding a gauge to the reinforcement included: grinding away the steel ribs at the desired

location to make a smooth bonding surface, cleaning and neutralizing the bonding area, gluing the gauge onto the surface, soldering the lead wires to the gauge, and covering the gauged area with a protective coating. The glue that was used was a moisture and chemical resistant two-part epoxy from Micro-Measurements (M-Bond AE-10). The protective coating was a thick two-part polymer compound also provided by Micro-Measurements (M-COATJ). Figure 25 shows a typical gauge bonded to the reinforcement before environmental protection was applied.

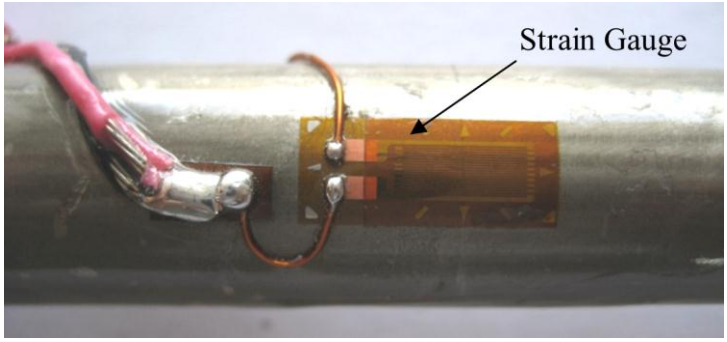

Figure 25: Strain Gauge Bonded to the Reinforcement before Environmental Protection

A Wheatstone bridge was utilized for detecting the changes in resistance in the strain gauges. More specifically, a “quarter bridge” arrangement was used and was constructed for each of the 16 strain gauge locations. As seen in Figure 26, one arm of a typical bridge was occupied by two strain gauges. The other three arms of the bridge were occupied by precision resistors with tolerances of ±0.01 percent purchased from Micro-Measurements Group. The arm containing the strain gauges was balanced by the 700 ohm resistance arm, which was made up of two precision resistors. The remaining two bridge arms each contained one precision resistor, each at 350 ohms.

The voltage applied to the circuit (E_{in}) was supplied by a single +5 V constant supply voltage regulator. The relationship between the output voltage (E_{out}) from the quarter bridge and the strain measured by the gauge was verified by performing a "shunt calibration". Shunt calibration consisted of connecting a large resistor of known value across the 700 ohm arm of the quarter bridge and the measuring the output voltage. This voltage was then compared with the expected voltage and corrected as necessary. Voltages were converted to strain values using the manufacturer's published gauge factor.

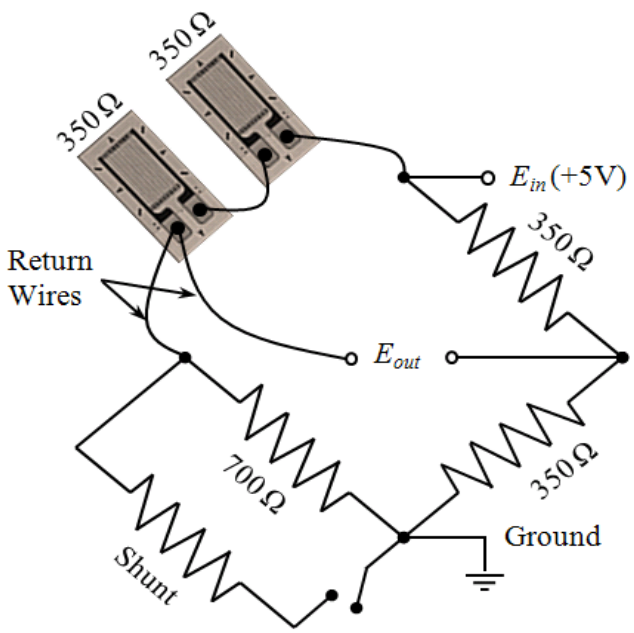

Figure 26: Quarter Bridge Strain Gauge Circuit Arrangement

In order to obtain axial strain measurements and not strains due to local bending within the gauged area, two gauges were used in the bridge arm of the quarter bridges. Having two strain gauges connected in series and symmetrically located about the neutral

axis of the rebar (top and bottom) allowed for the tensile (positive) strain due to bending in one gauge to be canceled out by the equal magnitude bending compressive (negative) strain in the other gauge. Two return wires of equal length were used in the quarter bridges (commonly referred to as a three-wire system) so that the resistance of the gauged arm would not be affected by the length of the lead wires.

Nine LVDTs with ranges of ± 0.125 inches were installed at various locations under the deck slab to capture deflection profiles for loads up to 100 kips in both the transverse and longitudinal directions (see Figure 27). In addition, one LVDT with a range of ± 1.0 inch was installed under the center point of the slab to measure the load-deflection response up to the ultimate failure load. Magnetic stands were used to hold the LVDTs in position throughout the test.

Figure 27: Photograph of LVDTs Under Test Slab

Data Acquisition

Readings from the strain gauges, LVDTs, and the load cell were recorded every five seconds during the test using a CR5000 data logger from Campbell Scientific, Inc. The panel containing the data logger and various supporting components and circuitry is shown in Figure 28. Signal conditioners were used in conjunction with the LVDTs to convert transducer mechanical position to an analog voltage reading. In order to accommodate all of the measurement channels needed for the test, one AM16/32 multiplexer was used in combination with the CR5000 data logger.

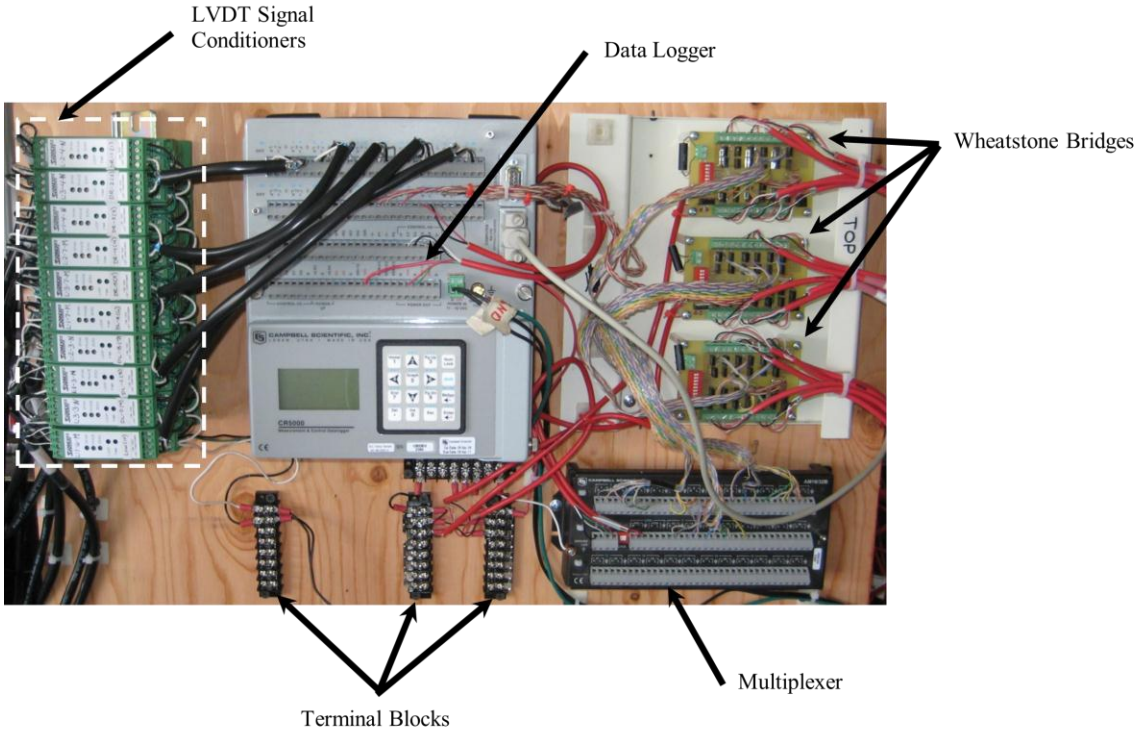

Figure 28: Components Within the Data Acquisistion Panel

ANSYS Finite Element Model

This section discusses all of the steps that were taken to create the FE bridge deck model in ANSYS. The steps taken to generate the nonlinear solution of the model are also explained. It should be noted that the bridge deck specimen was symmetric in geometry and loading about two vertical planes which permitted modeling of just one quarter of the slab and loading plate.

Element Types

A total of three different ANSYS element types were used in the model. The concrete was modeled with the Solid65 element, and all of the steel reinforcement was modeled with the Link8 element. The steel loading plate was modeled with the Solid45 element. The Solid65 and Link8 elements were previously introduced in Chapter 2; full descriptions of the element types are provided in the ANSYS element library (ANSYS, 2008).

Real Constants

ANSYS requires basic information, referred to as real constants, on certain properties of the elements to be used. These real constants are shown in Table 1 for each of the element types. A real constant set (RCS) was not created for the Solid45 element because one does not exist within ANSYS.

Table 1: Real Constants for the FEM Model

Real Constant Set (RCS)	**Element Type**	**Constants**	
1	SOLID65	All constants = 0 (no smeared properties)	
2	LINK8	Cross-sectional Area (in.^{2})	0.196
		Initial Strain (in./in.)	0.000
3	LINK8	Cross-sectional Area (in.^{2})	0.098
		Initial Strain (in./in.)	0.000
4	LINK8	Cross-sectional Area (in.^{2})	0.307
		Initial Strain (in./in.)	0.000
5	LINK8	Cross-sectional Area (in.^{2})	0.153
		Initial Strain (in./in.)	0.000

RCS 1 was used for the Solid65 element. The Solid65 element requires the input of real constants for up to three reinforcement bar materials to be smeared throughout the element. In this model, the discrete model method was used to model the reinforcement instead of the smeared model approach. Therefore, all of the real constants within the RCS 1 were set to zero to turn off the smeared reinforcement capability.

RCS 2, 3, 4, and 5 were used for the Link8 element. The Link8 element requires values for the cross-sectional area and initial strain in the element. RCS 2 and 3 were used for the #4 reinforcement while RCS 4 and 5 were used for the #5 reinforcement within the model. Two separate RCS were required for each type of reinforcement because of the symmetry that existed within the model. RCS 2 and 4 were used for the full cross-sectional area of the #4 and #5 bar respectively. Whereas, sets 3 and 5 were used for half of the cross-sectional area of the #4 and #5, bar respectively. Half cross-sectional areas were used to account for half of the rebar being bisected at mid-span

locations as a result of utilizing symmetry to model only one quarter of the slab. The initial strain was set to zero for all four real constant sets because no initial stress was applied to the reinforcement during testing.

Material Properties

In ANSYS, each of the element types required a material model set (MMS). MMS 1 was used for the Solid65 element. Both linear and multi-linear isotropic material properties were used to model the concrete. The linear isotropic material properties included the elastic modulus and Poisson's ratio. The elastic modulus (E_c) for the concrete was input as 5,053,393 psi, which was determined from tests on specimens from the deck panel concrete conducted at the time of the static load test. Poisson's ratio (υ) was assumed to be 0.15. As done by Wolanski (2004), the multi-linear isotropic material properties were input as five points from a compressive uni-axial stress versus strain curve developed by Kachlakev et al. (2001). The stress strain curve specific to this model is shown in Figure 29. The ultimate compressive strength (f'_c) was taken as 8,040 psi, which was the average concrete strength from cylinder tests conducted the day of testing.

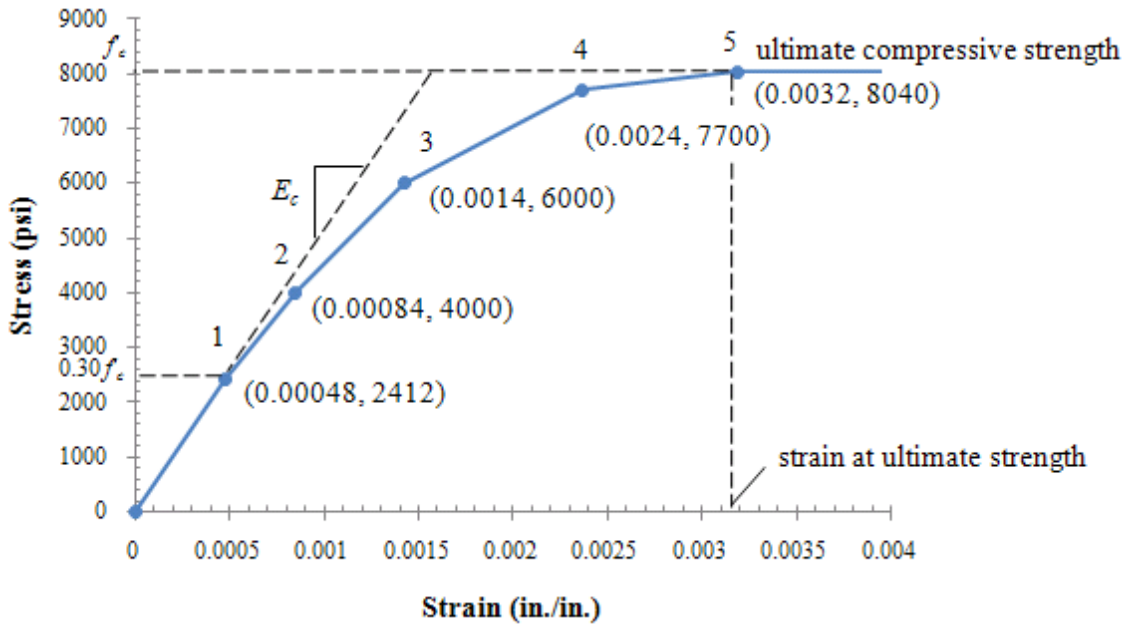

Figure 29: Compressive Uni-axial Stress Versus Strain Curve

MMS 1 also included cracking and crushing parameters to model the behavior of the concrete. As done in work by Wolanski (2004), the shear coefficient for an open crack was set to 0.3, and a coefficient of 1.0 was used for the closed crack. The uni-axial tensile failure stress was set to 766 psi. This value was based on the average tested modulus of rupture of the concrete on the day the panel was tested. To avoid convergence problems, the uni-axial crushing stress was input as -1 to turn off the crushing capability of the Solid65 element. Removing the crushing capability was not expected to impact the accuracy of the results due to the anticipated failure mechanism being punching shear which is a tensile rather than compressive based failure mechanism. Default values were used for the remainder of the input cracking and crushing parameters as recommended by Wolanski (2004). It should be noted that density was not added to this MMS, which in effect turned off the self-weight of the slab within the model. Self-

weight was not considered important because (a) the deflection due to self-weight was not measured by the LVDTs during the experimental test, and (b) the self-weight (4.8 kips) was not expected to substantially contribute to the total response of the test panel in punching shear under the center point load at failure, which was predicted to occur at a load in excess of 100 kips.

MMS 2 was used for the Link8 element to model the steel reinforcement. The rebar was modeled with both linear and bi-linear isotropic material properties. An assumed elastic modulus for steel (E_s) of 29,000,000 psi and Poisson's ratio (υ) of 0.3 were used. The bilinear properties entered included the yield stress (f_y) of 64,706 psi determined from tensile tests and an assumed hardening modulus of the rebar of 2,900 psi. The hardening modulus is also known as the tangent modulus and describes the plastic region of the stress-strain curve with a straight line. MMS 3 was used for the Solid45 element to model the steel loading plate. Since the steel plate was not expected to yield, the element only required linear isotropic material properties including the assumed elastic modulus (E_s) and Poisson's ratio (υ) for steel.

Modeling and Finite Element Discretization (Meshing)

The concrete slab and loading plate were modeled as volumes. Due to symmetry, one quarter of the slab and loading plate were modeled. The slab model was 27 inches wide, 50 inches long, and 6.5 inches thick. The loading plate was 5 inches by 10 inches by 2.5 inches. The density of the three-dimensional mesh needed to model the slab was determined by performing a convergence study. Five element densities (1500, 4875, 10,500, 19,500, 39,000) were used to examine the convergence of results of two

parameters. The parameters consisted of the mid-span deflection of the slab and the maximum top-surface tensile stress in the concrete. The results were taken at the same applied load and were based on linear analyses within ANSYS. As seen in Figure 30, the differences in results are insignificant when the number of elements increased from 19,500 to 39,000; therefore, the 19,500 element model was selected for this study. This mesh density corresponded to a rectangular concrete element size of 1 inch by 1 inch by 0.5 inch as seen in Figure 31.

The steel reinforcement was modeled as elements rather than lines to avoid having to create a line mesh. The existing mesh created from meshing the concrete volume allowed for individual Link8 elements to be inserted between concrete element nodes. Figure 32 shows the steel reinforcement configuration that was created within the concrete volume mesh. After all of the modeling parts were created, a merge command was utilized to join together the parts as one.

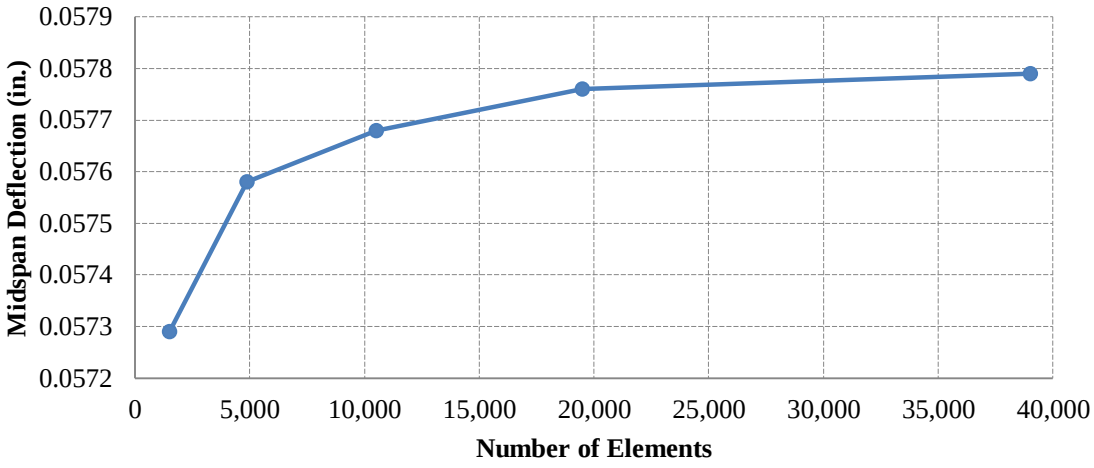

(a)

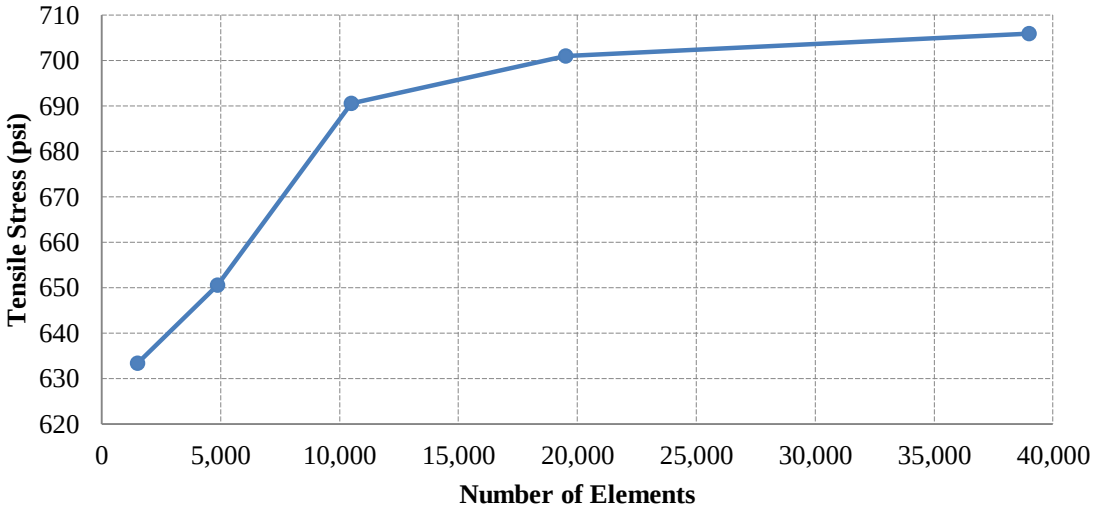

(b)

Figure 30: Convergence Study Results: (a) Deflection at Mid-span, (b) Tensile Stress in Concrete

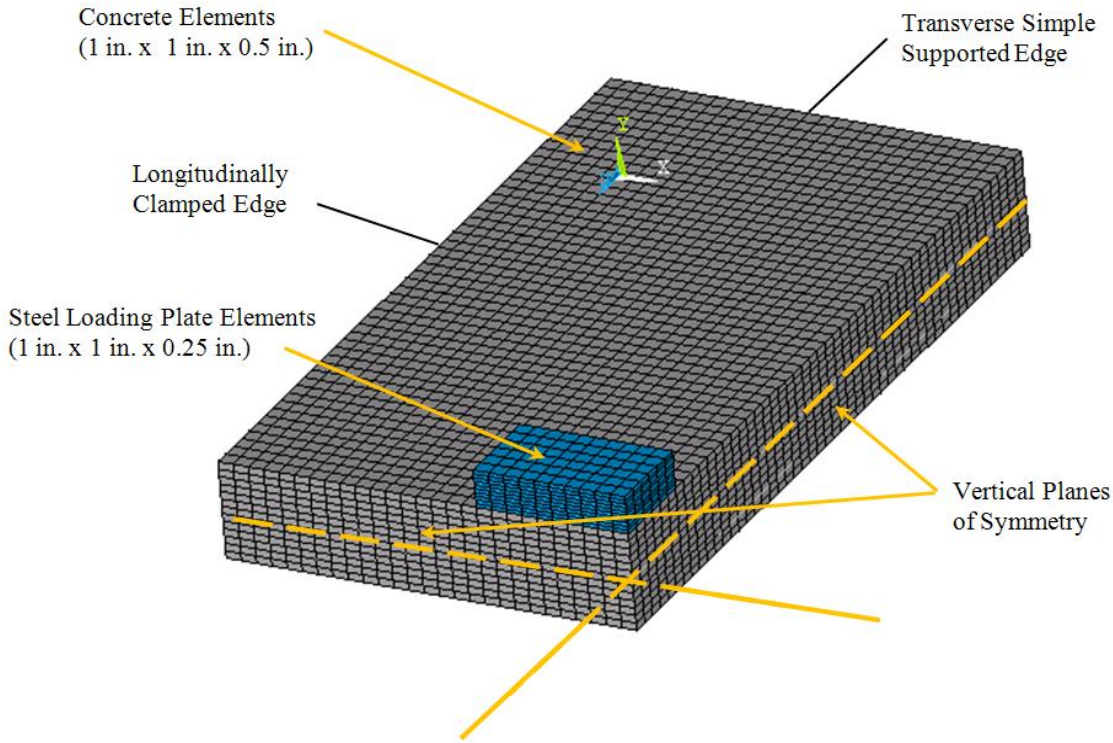

Figure 31: Mesh of the Concrete Slab and Steel Loading Plate

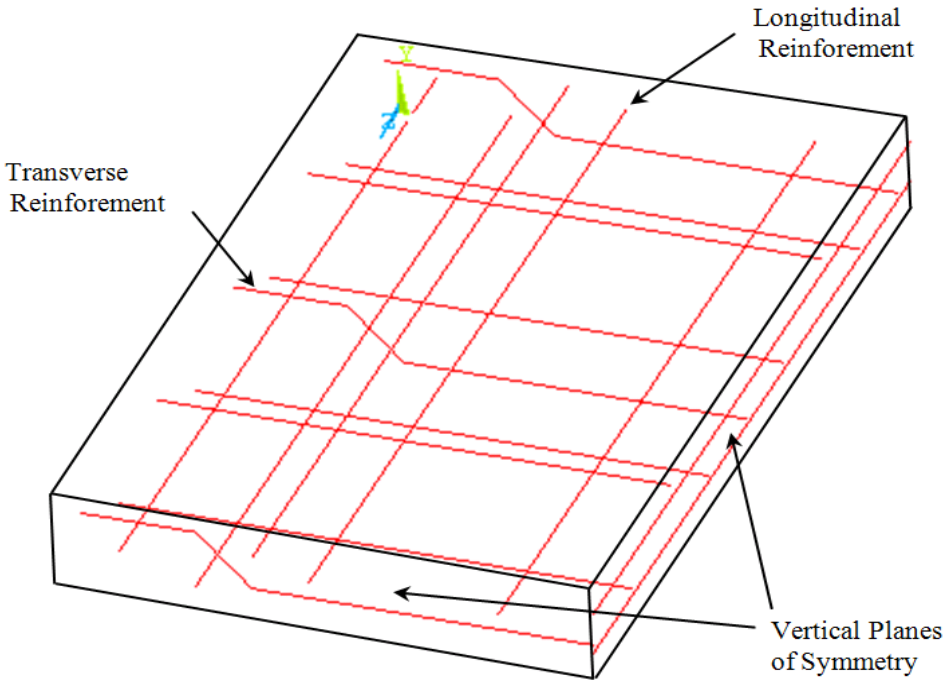

Figure 32: Steel Reinforcement Configuration

Loading and Boundary Conditions

In order to properly model the experimental set-up, loading and boundary conditions were applied to the FE model. Displacement boundary conditions were applied along the interior transverse and longitudinal edges to model symmetry. The nodes within both planes of symmetry were constrained from translation in the perpendicular direction to the plane. The effect of the test slab being clamped by the testing frame was modeled by fully constraining rotation and translation on the longitudinal exterior edge face of the FE model. A vertical nodal constraint along the bottom exterior transverse edge of the FE model was applied to model the beam support that was provided in this region during the test. The load was modeled as a uniform pressure over the top surface of the loading plate. The loading and boundary conditions for the FE model are shown in Figure 33.

Nonlinear Solution

The analysis type for the FE model was set to static with the assumption of small displacements. The nonlinear solution for the model was obtained by adjusting the solution controls. These controls were set to ANSYS default for loads within the linear range. For loads beyond the initiation of concrete cracking, convergence criteria had to be input. As recommended by past researchers (Kachlakev et al., 2001), the tolerances for convergence in force and displacement were set to five times the default values (0.5 percent for force checking, and 5 percent for displacement checking) in order to obtain convergence within the nonlinear solution steps.

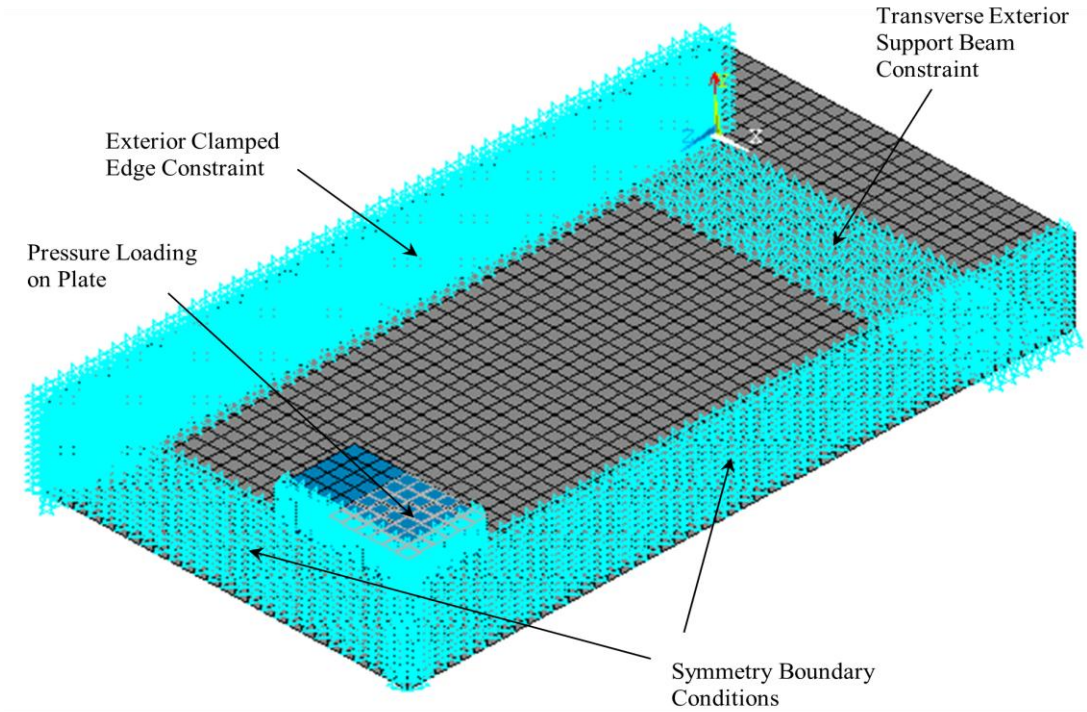

Figure 33: Boundary and Loading Conditions for FE Model

The nonlinear analysis was performed using the Newton-Raphson option. This option required the application of the load to be broken down into incremental steps. A batch file containing basic code was created to incrementally apply load to the FE model and record all solutions up to failure. The load step sizes were specified within the batch file and varied in size based on ease of convergence. In the linear range of the model where convergence was easy to obtain, the load step size was set to 10,000 pounds. In solution steps where convergence became difficult, such as initial cracking of the concrete and approaching the ultimate failure of the model, the load increments were set to as low as 5 pounds. Failure of the FE model was defined when the solution could no longer converge at the smallest load step setting.

CHAPTER 4 - ANALYSIS AND DISCUSSION OF RESULTS

Introduction

This chapter presents the results of the static load test performed on a full-scale bridge deck specimen as well as the related findings from the FEA. The results are presented in terms of cracking behavior, deflection histories, strain measurements in the steel reinforcement, ultimate capacity, and mode of failure. The results are discussed and used to validate the effectiveness of the laboratory testing frame in obtaining the desired stress conditions within the test slab. In addition, a fatigue life model is used to assess the reasonableness of loading an identical test panel to failure with an accelerated rolling wheel load.

Results from the Laboratory Investigation and Finite Element Analysis

The first section of this chapter provides the results from the experimental study and the FEA. Results for the ultimate capacity of the slab are then compared to those determined by hand calculations.

Cracking Behavior

Prior to loading, the test slab had one top surface diagonal crack that formed as the specimen was bolted into the reaction frame. The crack ran across the entire specimen in the transverse direction perpendicular to the supporting beams. The first top surface cracking during the physical test occurred at a load of approximately 30 kips. The cracking load for the FE model was approximately 39 kips, which is 30 percent

higher than the experimental results. First cracking loads obtained from ANSYS reinforced concrete models have been reported to be higher than experimental data in work done by both Kachlakev et al. (2001) and Wolanski (2004). One reason for this discrepancy as explained by Kachlakev et al. (2001) is that the ANSYS models do not consider the existence of microcracks in the concrete.

Throughout the duration of the physical test, cracks were mapped on the entire top surface of the test slab. For the FE model, crack patterns were recorded at each applied load step. Figure 34 shows the evolution of top surface crack patterns for the experimental test slab at six different load levels: 30, 75, 100, 125, 150, and 175 kips. As seen in the figure, the first top surface cracks appeared along the longitudinal edges of the slab, adjacent to the girders. With increased load, subsequent cracks formed and propagated in semicircles around the loaded area. Note that the top surface crack that formed prior to loading is shown as a dashed line.

The top surface cracking behavior was confirmed by the ANSYS model, with longitudinally oriented cracks initiating in the negative bending moment regions of the slab which propagated into a circular crack pattern around the loaded area at higher loads. In Figure 35, the top surface crack pattern obtained from the FEA at the last converged load step is compared to a photograph of the test slab after failure. In ANSYS, cracks are displayed as circle outlines in the plane of the crack. Due to the fact that all of the cracking occurred in the vertical plane of the slab, the cracks appear as line segments in Figure 35. Cracks can occur at eight different integration points in each concrete element. A red circle indicates the first crack at an integration point. Figure 35 shows

that the FE model reasonably predicted the top surface crack pattern of the experimental slab with a majority of cracks forming along the sides of the support channels and the remaining cracks forming a circular pattern around the loaded area.

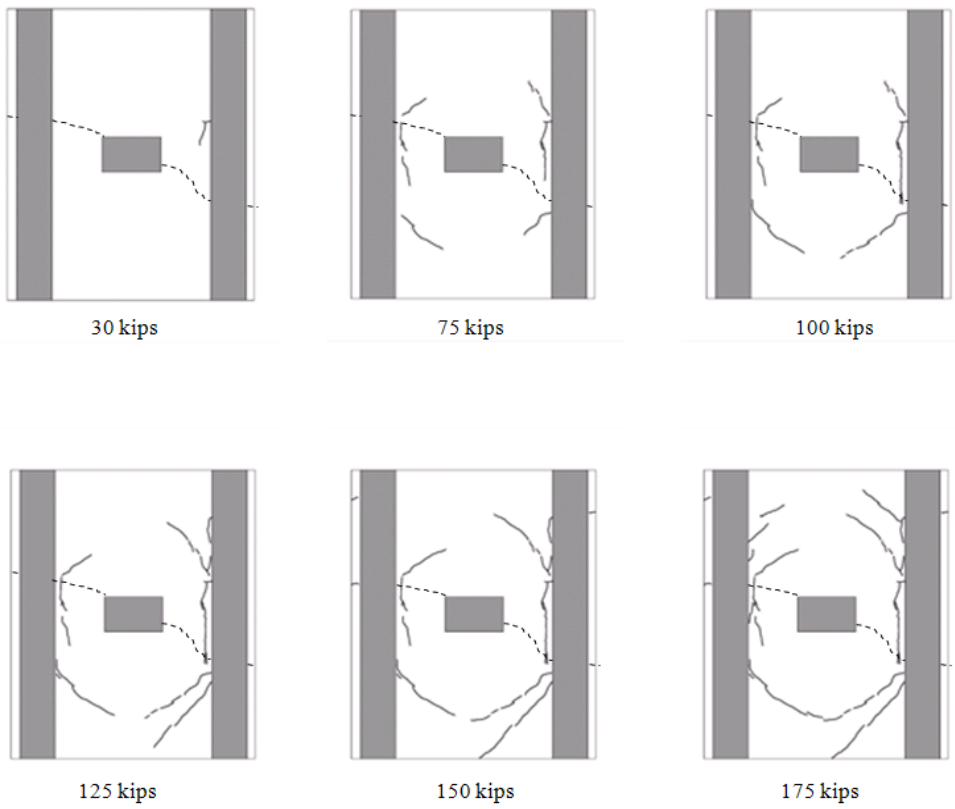

Figure 34: Evolution of Crack Patterns on Top Surface of Test Slab

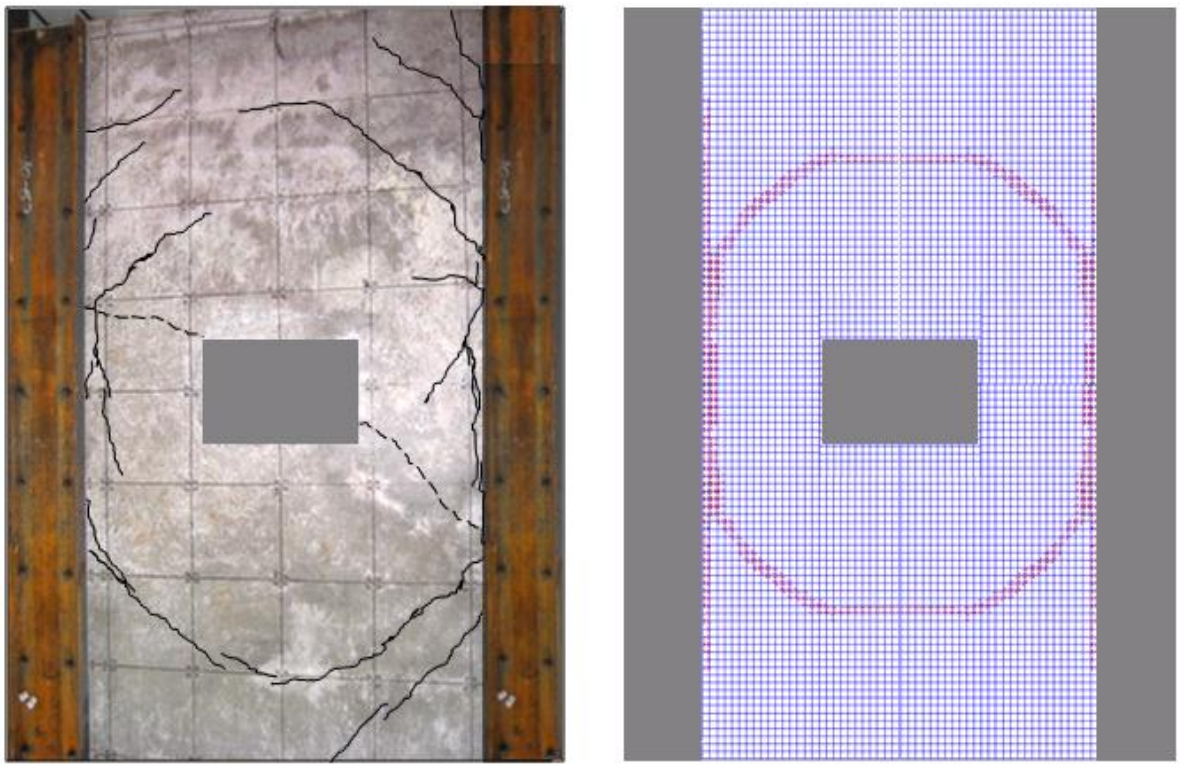

(a) (b)

Figure 35: (a) Experimental Results, (b) ANSYS Model Prediction

Ultimate Capacity and Mode of Failure

The test slab failed abruptly in punching shear around the loaded area. The punching failure in the top surface had an elliptical shape that passed through the corners of the loading area. The bottom failure surface generally was square in shape with a side dimension approximately equal to the full span in the transverse direction. The top surface and the quarter of the bottom surface that was mapped for cracks are shown in Figure 36. Similar failure patterns were observed in static load tests performed by El-Gamal et al. (2005). The failure load for the test slab was 192 kips. The final load from the FEA indicated by unattainable convergence was 176 kips, which is lower than the

actual ultimate load by 8 percent. In the past work done by Kachlakev et al. (2001), the ANSYS reinforced concrete models underestimated the ultimate strengths obtained experimentally for all tests performed.

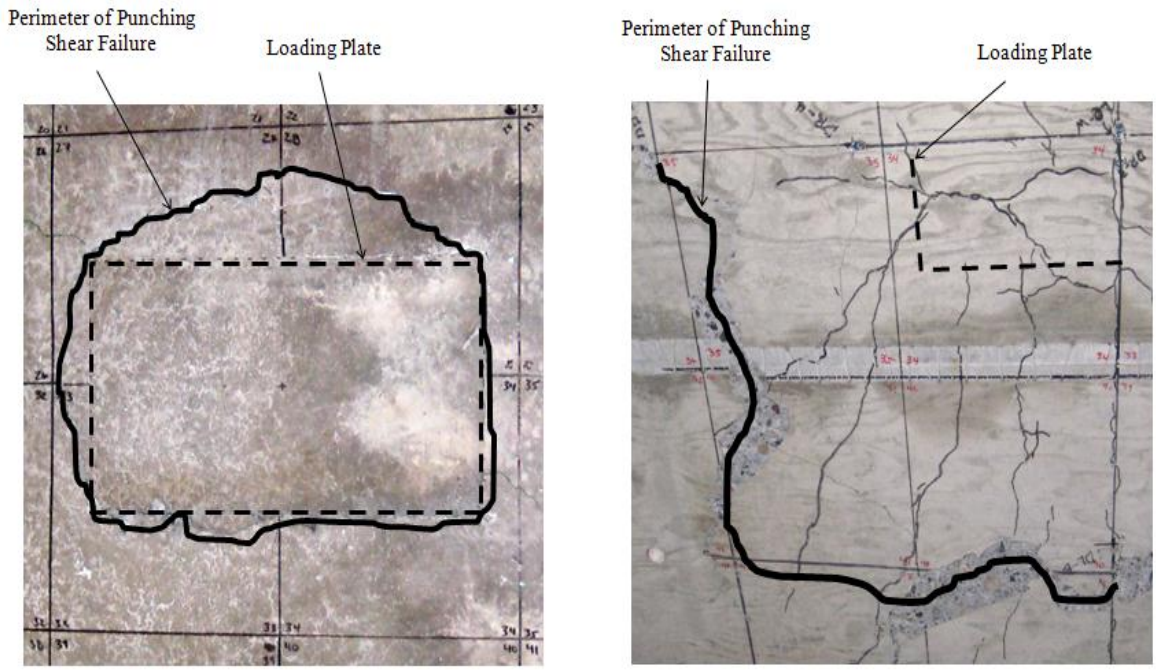

(a) (b)

Figure 36: Photographs of Punching Shear Failure (a) Top Surface, (b) Bottom Quarter Surface

Load-Deflection Plots

The deflection at the center point of the test slab was measured up to the ultimate failure load. The load-deflection plot from the experimental results and the FE model are shown in Figure 37. Note that the regular “drops” in the experimental plot at each load step appear to be the result of creep in the concrete (Bazant, 2012). The overall deflection behavior of the test slab was consistent with that described by El-Gamal et al. (2007).

Referring to Figure 37, the experimental load-deflection curve shows a well defined elastic and plastic region, as was expected. The load-deflection plot generated from the FEA is significantly stiffer than that obtained from the experimental results. The ANSYS load-deflection plot in the linear range was stiffer than that from the experimental results by approximately 68 percent. The two plots have similar trends after first cracking; however, the ANSYS model is stiffer than the experimental slab by approximately 30 percent. Kachlakev et al. (2001) also reported that the finite element model was stiffer than the actual beam for all beams tested. It was concluded in the ANSYS modeling work done by Ibrahim and Mahmood (2009) that there are two main factors that cause the higher stiffness in ANSYS reinforced concrete finite element models. One reason is that the ANSYS finite element model assumes that the bond between the concrete and reinforcing steel is perfect, i.e., no slip occurs. The other factor, as stated previously, is that the ANSYS finite element model does not incorporate the existence of microcracks produced by drying shrinkage and handling. Another explanation for the physical model being less stiff than the ANSYS model is the possibility that the testing frame did not provide perfectly clamped edge conditions. However, in later discussion in this chapter, evidence is presented that fixity was maintained in the longitudinal edges of the test panel, and this difference in stiffness apparently is an artifact of the FEA, as other investigators have observed.

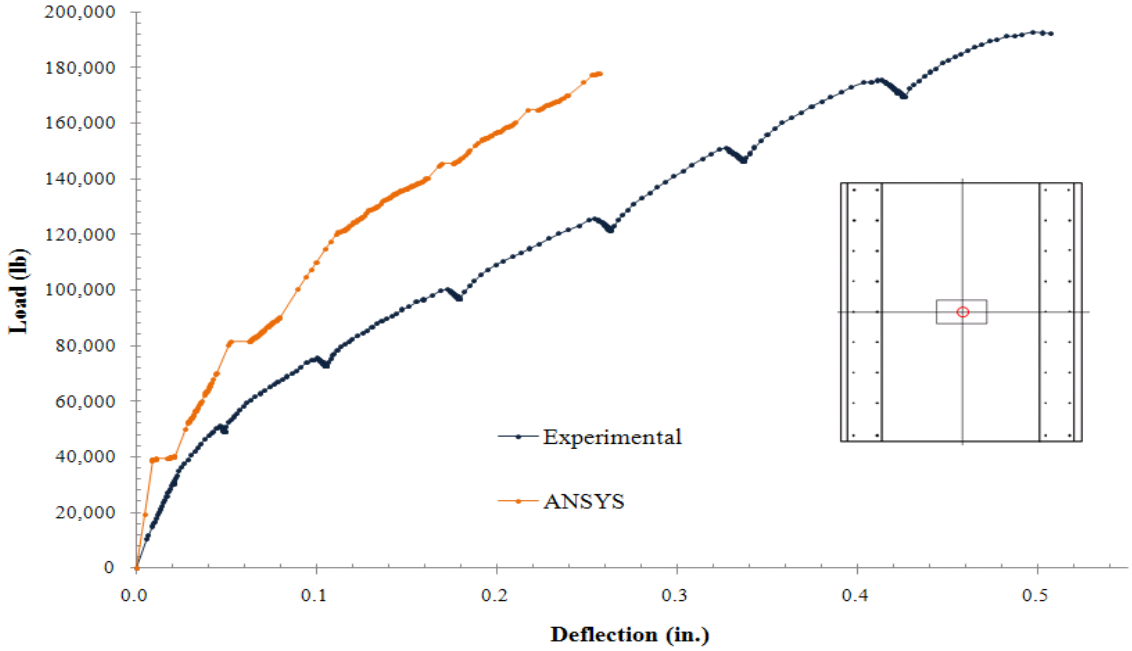

Figure 37: Load-Deflection Plot for Test Slab

Deflection profiles were generated from deflection measurements taken at five locations along both the transverse and longitudinal directions of the test slab. Profiles were captured experimentally for five different load levels including: 20, 40, 60, 80, and 100 kips. These profiles are presented in Figure 38 and Figure 39. The deflection profiles were consistent with those described by El-Gamal et al. (2007). In the transverse direction, the deflected shapes resembled that of shallow cones. While reversed curvature consistent with clamped edge behavior is not pronounced in these profiles, insufficient data was collected (quarter points only) to fully characterize the deflected shapes. In the longitudinal direction, deflections were more concentrated around the loaded area. The general deflected shapes were confirmed by the FE model. However, the magnitudes of the deflections were significantly lower due to the ANSYS model being so much stiffer than the actual test slab.

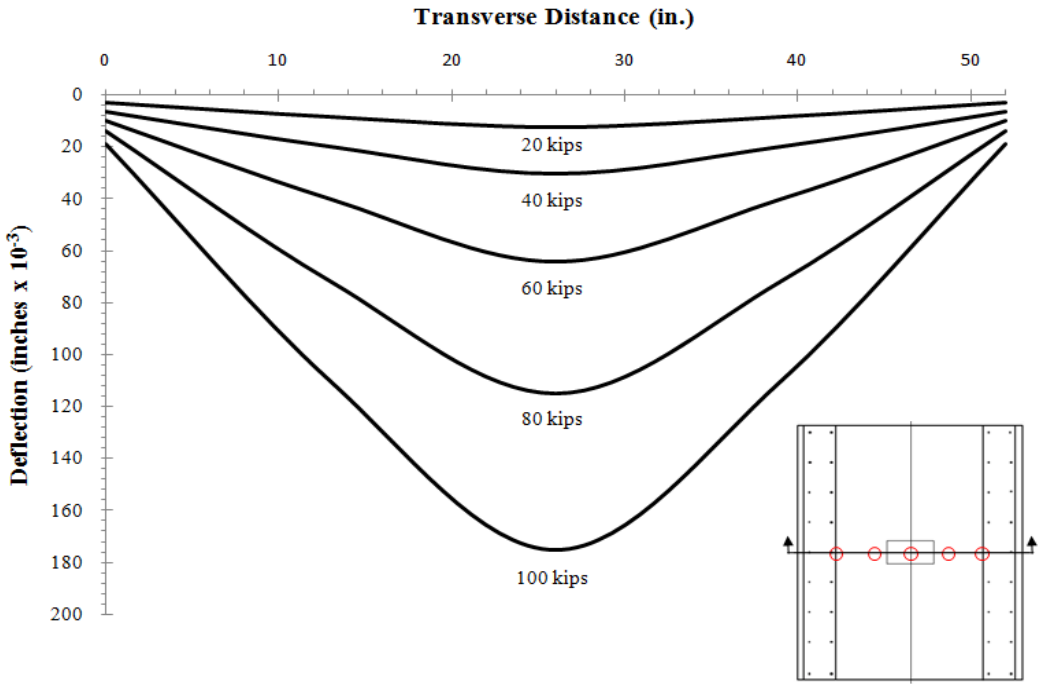

Figure 38: Experimental Deflection Profile along Transverse Direction of Slab at Various Load Levels

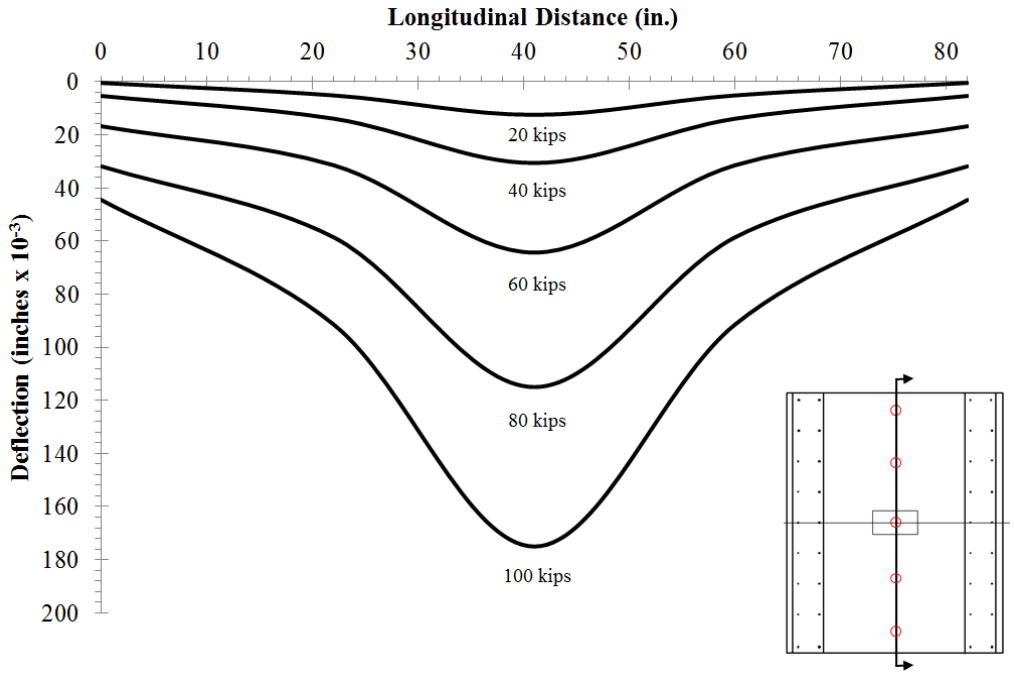

Figure 39: Experimental Deflection Profile along Longitudinal Direction of Slab at Various Load Levels

Load-Strain Plots

Strains were measured in the top and bottom reinforcing bars at four locations along both the transverse and longitudinal centerlines of the test slab. Along each centerline, the gauges were symmetrically placed in pairs, with two pairs per line (see Figure 24). A single load-strain plot was produced for each symmetric gauge location by averaging the data collected at the paired sites. The resulting strain responses are presented in Figure 40 through Figure 43. Again, note that the regular drops in the response are attributed to creep in the concrete at each load step. These strains were compared to the results obtained from the FE model at an extreme upper expected load level to be used for future fatigue tests of 40 kips. This load was above the cracking load of both the FEA and physical models, and was also expected to conservatively challenge the rotational fixity offered along the longitudinal edges of the test panel well beyond that required at an operating load level of 15 kips.

Transverse Direction. As seen in Figure 40, at the mid-span location in the transverse direction, tensile strains (positive values) exist in the bottom of the deck and compressive strains (negative values) exist in the top of the deck for loads up to about 85 kips. These strains are generally consistent with the expected positive bending moment and observed deflected shape at the mid-point of the slab. At the 40 kip load level, a tensile strain of 473 micro-strain and a compressive strain of 116 micro-strain were recorded. At the same load level (which is slightly above the first cracking load predicted in ANSYS of 39 kips), the ANSYS model predicted a tensile strain of 452 micro-strain,

and a compressive strain of 123 micro-strain. These tensile and compressive strains were higher than the experimental results by 4 and 6 percent, respectively.

Referring to Figure 41, at the edge locations in the transverse direction, compressive strains exist in the bottom of the deck and tensile strains exist in the top of the deck for loads up to 75 kips. These strains are consistent with the expected negative bending moment and deflected shape at the edge locations of the slab. At the 40-kip load level, a tensile strain of 30 micro-strain and a compressive strain of 37 micro-strain were recorded. At the same load level, the ANSYS model predicted tensile and compressive strains of 35 and 46 micro-strain, respectively. These tensile and compressive strains were higher than the experimental results by 17 and 23 percent, respectively.

Longitudinal Direction. As seen in Figure 42, at the mid-span location in the longitudinal direction, tensile strains exist in the bottom layer of reinforcement and compressive strains exist in the top layer of reinforcement for loads up to 100 kips. These strains are consistent with the expected positive bending moment and deflected shape at the mid-point of the slab. At the 40 kip load level, a tensile strain of 129 micro-strain and a compressive strain of 242 micro-strain were recorded. At the same load level, the ANSYS model predicted tensile and compressive strains of 174 and 268 micro-strain, respectively. These tensile and compressive strains were higher than the experimental results by 35 and 11 percent, respectively.

Referring to Figure 43, at the edge locations in the longitudinal direction, compressive strains exist in the bottom layer of reinforcement and tensile strains exist in the top layer of reinforcement. These strains are consistent with the deflected shape at

the edge locations of the slab. At the 40 kip load level, a tensile strain of 7 micro-strain and a compressive strain of 24 micro-strain were recorded. At the same load level, the ANSYS model predicted a tensile strain of 19 micro-strain and a compressive strain of 15 micro-strain. This tensile strain was higher than the experimental results by 62 percent. This compressive strain was lower than the experimental results by 36 percent.

Discussion. All of the natures of the strains (i.e., tensile or compressive) were confirmed by the ANSYS model at the 40 kip load level. In general, at this load level, the strains in the steel reinforcement for the ANSYS model were higher than those found experimentally. ANSYS model strains being consistently higher than the experimental strains was also observed in work done by Kachlakev et al. (2001). It should be noted that the strains predicted by ANSYS matched more closely the experimental results for the transverse direction of the slab than those predicted for the longitudinal direction, and that the focus of this project is on stress conditions in the transverse direction.

Comparison of Predicted and Observed Ultimate Capacity

The punching capacity of the test slab was predicted using the ACI 318-08 code equation (ACI 2008), and two modifications to the code equation provided by Graddy et al. (2002) and El-Gamal et al. (2005). Both modifications attempt to compensate for compressive membrane forces that develop when a concrete slab is restrained, and yield higher capacity predictions than those provided by the ACI code equation.

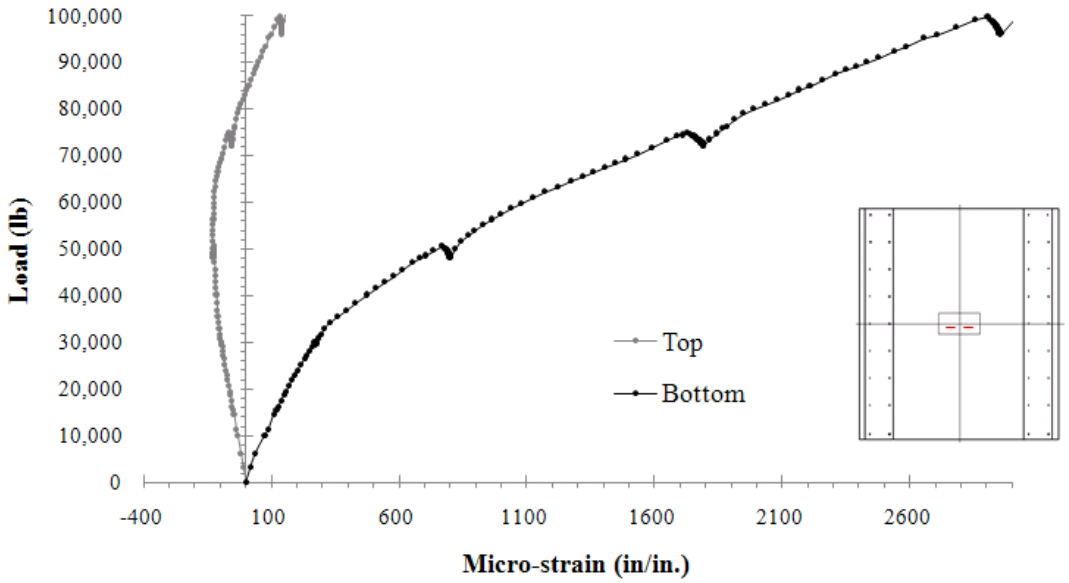

Figure 40: Load-Strain Plots for Mid-span Top and Bottom Reinforcement in Transverse Direction

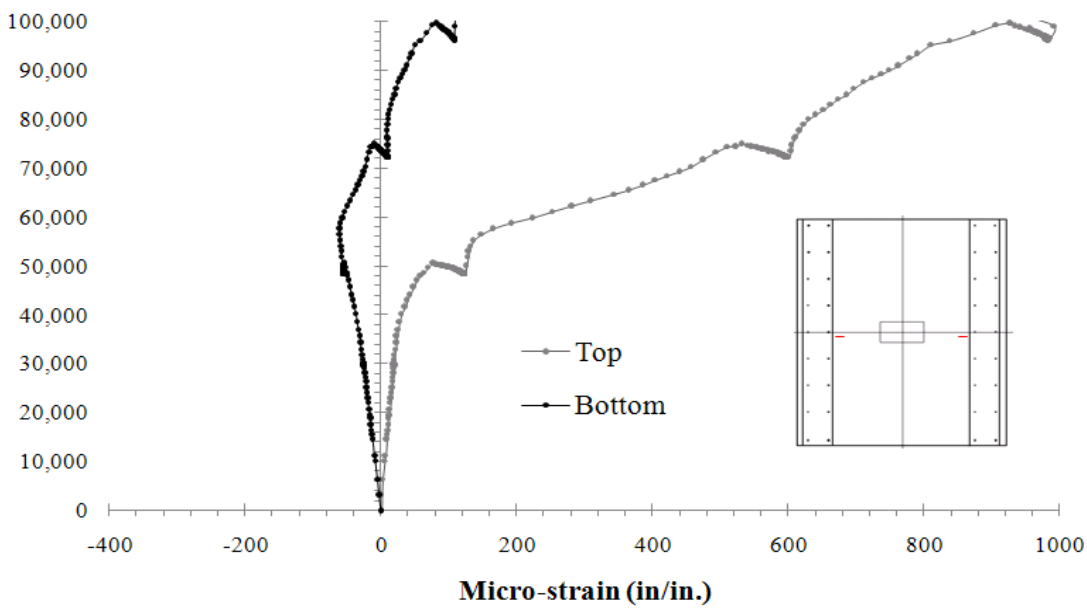

Figure 41: Load-Strain Plots for Edge Top and Bottom Reinforcement in Transverse Direction

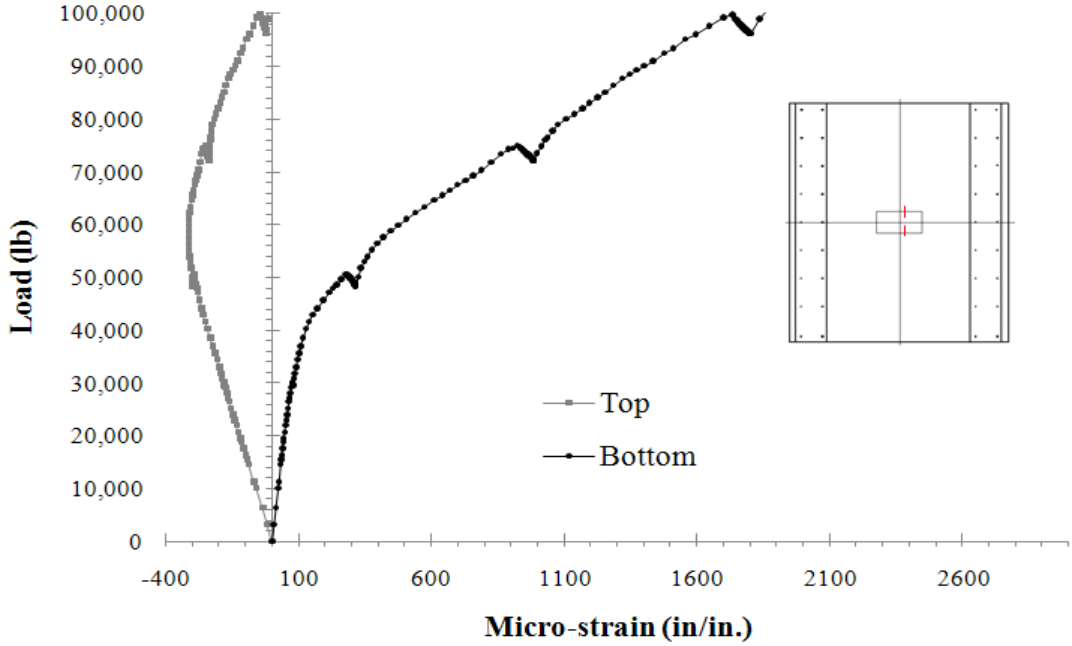

Figure 42: Load-Strain Plots for Mid-span Top and Bottom Reinforcement in Longitudinal Direction

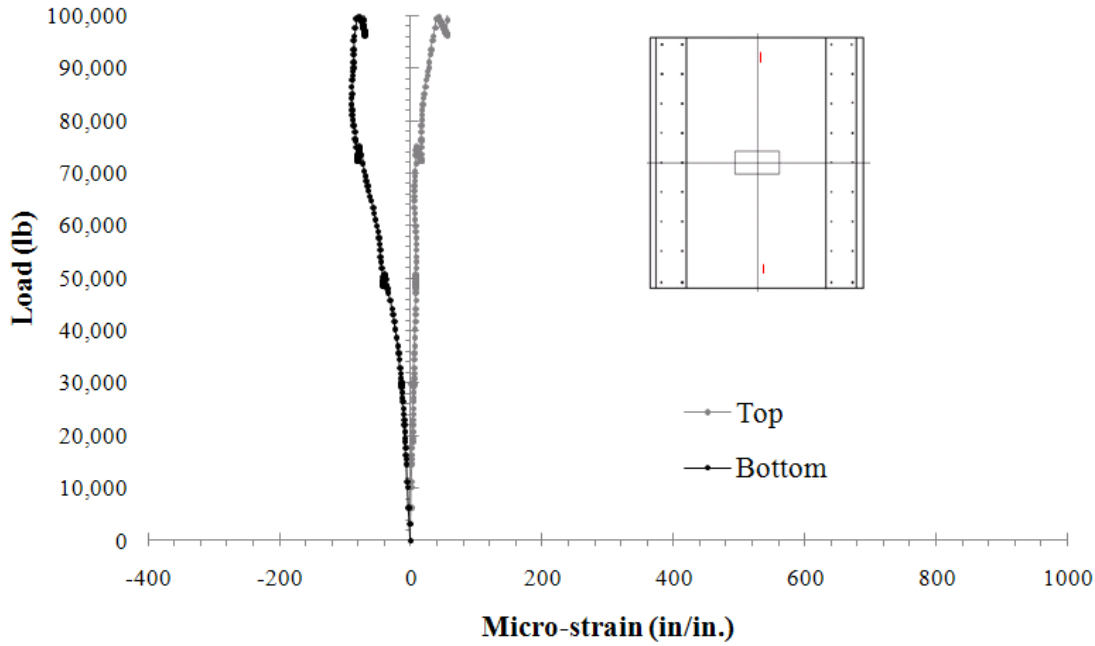

Figure 43: Load-Strain Plots for Edge Top and Bottom Reinforcement in Longitudinal Direction

The ACI code equation (11.11.2.1) for the punching shear capacity associated with a rectangular loading footprint in non-pre-stressed slabs can be expressed as follows:

$$V_c = \left(2 + \frac{4}{b_2/b_1}\right)\sqrt{f'_c}\,b_o d \le 4\sqrt{f'_c}\,b_o d$$

Equation 16

where b_1 and b_2 represent the dimensions of the rectangular loading plate and the remaining variables are as defined previously. The ACI punching capacity was determined to be:

$$V_c = 4 \times \sqrt{8040} \times 2\left(\left(2 \times 4.88\right) + 12 + 20\right) \times 4.88 = 146{,}183 \text{ lb. (146 kips)}$$

Equation 17

The predicted shear capacity was then calculated using the modified equations for restrained concrete slabs developed by Graddy et al. (2002). This prediction assumed an idealized conical failure surface with the same angle of inclination on each of the four sides of the perimeter around the loaded area. As depicted in Figure 44, the angle of the inclined conical failure surface to the horizontal (θ) was assumed to be 38 degrees. Using Equation 3 and Equation 4, the predicted shear capacity was calculated to be:

$$V_c = 2\left(12 + 20 + \frac{2 \times 4.88}{\tan(38)}\right)\frac{4.88}{\tan(38)} \times 4\sqrt{8040} = 199{,}348 \text{ lb. (199 kips)}$$

Equation 18

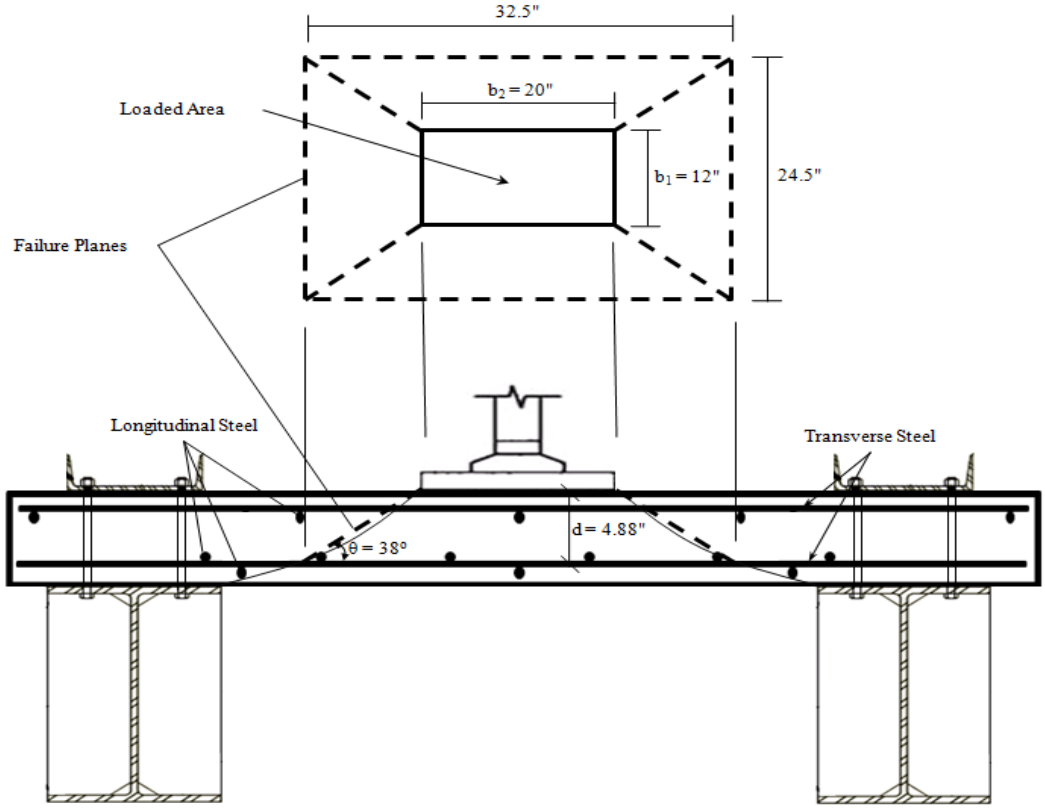

Figure 44: Assumed Failure Planes for Test Specimen

The punching capacity was also predicted using the equations developed by El-Gamal et al. (2005). Using Equation 5 and Equation 6 with the assumption of maximum possible slab restraint, the shear capacity was predicted to be:

$$V_c = 0.33 \times \sqrt{55.4} \times 2((2 \times 124) + 305 + 508) \times 124$$
$$\times \left[0.62(0.0062 \times 200)^{1/3} \left(1 + \frac{8 \times 124}{2((2 \times 124) + 305 + 508)} \right) \right] \times 1.2^2 = 909{,}712 \text{ N (205 kips)}$$

Equation 19

Table 2 provides a summary of the ultimate capacity predictions and the percent differences from the experimentally found capacity of 192 kips. As seen in Table 2, the

actual punching shear capacity of the test slab was considerably higher (24 percent) than the ACI code prediction. The prediction from Graddy et. al. (2002) was within 4 percent of the actual capacity while the El-Gamal et al. (2005) equation prediction was within 6 percent.

Table 2: Summary of Ultimate Capacity Predictions

Prediction Method	**Predicted Ultimate Capacity (kips)**	**Percent Difference from Observed**
ACI 318-08	146	24%
Graddy et al.	199	4%
El-Gamal et al.	205	6%
ANSYS	176	8%

Validation of the Laboratory Testing Frame

This section discusses a main objective of this study, which was to verify the ability of the laboratory support frame to generate the desired stress response for testing full-scale bridge deck panels. In order to capture realistic transverse bridge deck stresses, the laboratory testing frame needs to provide those boundary conditions on full-scale test slabs that were assumed in the investigation performed by Stordahl (2009). These boundary conditions include fully clamped conditions along the longitudinal edges and simple support conditions along the transverse edges of a test slab. The experimental data from the static load test and supporting FE model results provides a means to verify that the support frame can provide the required boundary conditions needed for future fatigue testing.

The ability of the support frame to provide the restrained conditions needed for future testing was indicated by the existence of the expected distribution of flexural stresses within the test slab during the static load test. As described previously, these stresses consist of transverse tensile stresses in the top surface of the deck near the face of the supports, and transverse compressive stresses in the top of the deck at the mid-span. The observed crack patterns in the test slab were consistent with the expected distribution of stresses during the static load test. All of the top surface cracks initiated along the face of the supports, and bottom surface cracks were concentrated directly under the applied load.

As expected, the internal strain measurements in the transverse direction of the test slab were tensile in the bottom of the deck and compressive in the top at mid-span. The strains measured near the clamped edges were tensile in the top of the deck and compressive in the bottom for loads up to 75 kips. This indicates that the desired reverse moment behavior in a test slab is achievable using the support frame at the 15 kip load level to be used for future testing. A further indication that the testing frame provided the degree of fixity needed for testing is that the measured strains in the transverse direction closely matched those obtained in the FE model which assumed full rotation and translation restraint. Negligible strains were measured in the longitudinal direction at the 40 kip load level at the transverse edges, indicating the existence of simple support conditions at these locations. The fact that the ultimate capacity predictions for restrained reinforced concrete slabs more closely matched the experimental result than the ACI code prediction, which does not take into account slab edge restraint, was more evidence that

the testing frame can provide the desired restraint at the longitudinal edges of the test slabs.

Fatigue Life Model Predictions

Another important objective of this study was to estimate the number of cycles needed to fatigue a test sample to failure with a moving wheel load. The expected maximum applied load for future testing is up to 30 kips. As described previously, Matsui et al. (2001) developed a fatigue life relationship in which the number of load cycles to failure is expressed as a function of the applied load divided by the ultimate capacity of the deck slab (Equation 1). In this model, the ultimate capacity of the deck slab is its punching shear capacity, which from the static load test was found to be 192 kips. However, the tested slab was constructed with significantly stronger concrete (8,040 psi on test day) than that to be used in future specimens (4,000 psi). Based on the punching shear capacity equations (i.e. Equation 19), slab failure load is a function of the square root of the concrete's compression strength. Therefore, the expected failure capacity of the slabs to be tested is 70 percent of the 192 kip capacity found experimentally, which equates to 134 kips. Similarly, the expected cracking load of the slabs to be tested is 21 kips (i.e. 70 percent of the observed cracking load of 30 kips). At load levels above the cracking load, a significant reduction in fatigue life is expected based on Petrou et al. (1994) observations in their rolling wheel load tests.

Before moving ahead and applying the fatigue life equation of Matsui et al. (2001), further consideration was given to the appropriate ultimate capacity of the deck slab to be used in this equation. The focus of future work in this program is on deck

rehabilitation methods that will be applied well before full structural failure. Therefore, in applying the equation developed by Matsui et al. (2001), it seemed inappropriate to simply use the ultimate load carrying capacity. Rather, one approach would be to use as the terminal condition in this relationship the point at which a surface treatment is no longer a viable rehabilitation strategy rather than the ultimate structural capacity. While this serviceability failure point will be reached prior to the punching shear capacity, the specific load level at which it will be reached is unknown. Only limited research was found to assist in defining a serviceability failure point. Huang et al. (2004) performed an analysis of life-cycle maintenance strategies for concrete bridge decks and suggested that the maximum tolerable condition index at which deck treatments are still effective is 35, on a scale of 0 to 100. That being said, the correspondence between this condition index, fatigue damage, and structural capacity is unknown. Nonetheless, as a starting point, it was assumed that a serviceability failure point of 35 on a scale of 100 can be represented in the fatigue life equation simply as 35 percent of the monotonic failure load (in this case, 35 percent of 134 kips, or 47 kips). Such an assumption offers some basis for evaluating the proposed modified implementation of Matsui's fatigue life equation. This assumption also passes at least one simple and critical test of reasonableness, that is, as the maximum tolerable index increases, so does the predicted fatigue life.

Various applied load levels were considered in Matsui's equation, with the resulting predicted fatigue lives presented in Table 3. As outlined above, the ratio P/P_s was taken as the applied load divided by the assumed serviceability failure point (35 percent of 134 kips). Time to failure is also shown in Table 3, assuming the test machine

to be used will be capable of applying 32,000 cycles per week (Stordahl, 2009). As can be seen in Table 3, the results are extremely sensitive to the assumed applied load. Specifically, at an operating load level of 15 kips, which is below the expected cracking load of the test slabs (21 kips), over 400 billion cycles are required to deteriorate the deck slabs, which is obviously impractical. When the applied load is increased to above the expected cracking load, the number of cycles to failure is sharply reduced and testing times become feasible. This situation is consistent with the findings of Petrou et al. (1994) in their rolling wheel load tests when the applied load exceeded the slab cracking load. These results indicate the importance of fatigue testing at a load above the cracking load of the deck slabs, or possibly the need to pre-crack the slabs if lower load levels are to be used (as was done in the investigation performed by El-Ragaby et al. (2007)).

Table 3: Fatigue Life Predictions for Bridge Deck Test Specimens

Applied Load *P* (kips)	P/P_s	***N***	**Time (months)**
15	0.32	436,274,359	3,408
22	0.47	3,287,241	25.7
23	0.49	1,893,954	14.8
24	0.51	1,082,747	8.5
25	0.53	643,058	5.0
26	0.55	389,807	3.0
27	0.58	240,799	1.9
28	0.60	151,380	1.2
29	0.62	96,729	0.8
30	0.64	62,754	0.5

CHAPTER 5 - CONCLUSIONS AND RECOMMENDATIONS

This chapter summarizes the major findings of the experimental study and finite element analysis performed to fulfill the three main objectives of this study, which consisted of:

1. designing a support frame for the purpose of fatigue testing full-scale models of concrete bridge deck panels under a rolling wheel load,
2. validating the performance of this support frame relative to replicating selected stress environments consistent with those in real bridge decks under vehicle loads, and
3. predicting the number of cycles needed to deteriorate a test panel under a given moving wheel load.

This chapter also provides recommendations for the research study set out by WTI to evaluate the performance of bridge deck rehabilitation strategies. In addition, suggested recommendations are made for future research pertaining to finite element modeling of the reinforced concrete bridge deck specimens in ANSYS.

Summary

A laboratory testing frame that supports multiple full size bridge deck specimens for the purpose of fatigue testing was designed and constructed in this effort. The frame was designed to provide fully clamped conditions along the longitudinal edges, and simple support across the leading and trailing edges of each test specimen. The frame was also designed to provide sufficient access to the underside of each deck panel to

install instrumentation and to visually inspect the bottom surface of the panels for progressive damage during testing. The frame consists of longitudinal and transverse W24 beam sections that support the edges of the test panels. Rotation of the longitudinal edges of the panels is prevented by clamping them between the top flange of the W section and a channel section laid on top of the panels using a double row of bolts. Further, frequent web stiffeners were added to the longitudinal W sections to enhance their torsional stiffness and thus better maintain a fixed edge condition along the edges of the slabs.

Following design and construction of the frame, a static load test was conducted on a single bridge deck specimen to confirm its performance. Important findings of this test were:

1. Top surface cracks initiated in the deck panel along the face of the longitudinal supports, and bottom surface cracks formed directly under the applied load indicated that the support frame provided the desired fixity along the longitudinal panel edges.
2. Internal strain measurements in the transverse direction of the test slab at mid-span found tensile strains in the bottom of the slab and compressive strains in the top of the slab consistent with positive transverse moment. Conversely, transverse strains at edge locations were compressive in the bottom of the deck and tensile in the top of the deck consistent with negative transverse moments. These strain measurements further validated that the support frame produced the desired reverse moment behavior consistent with fixity of the longitudinal edges

of the panel. The degree of this fixity was confirmed by comparing the magnitude of the measured strains with those strains predicted in an FE model which assumed fully fixed panel edges.

3. The punching shear failure load exceeded that predicted by the ACI 318-08 code equation by 32 percent, but was within 4 and 6 percent of the predicted capacities using equations that take into account restrained slab conditions provided by Graddy et al. (2002) and El-Gamal et al. (2005). These results further indicate the degree of edge restraint provided by the support frame.
4. In the longitudinal direction of the test slab, as expected, internal strain measurements were tensile in the bottom of the slab and compressive in the top of the slab for the mid-span location under a 40 kip load. At the edge locations in the longitudinal direction, the strains under a 40 kip load were almost zero, indicating that the testing frame supplied the desired simple support conditions along the transverse edges of the slab. This simple support condition was also confirmed in the longitudinal deflection profile for the 40 kip load.

Additional observations on the performance of the FE model that supplemented the experimental study include:

1. The first top surface cracking load predicted by the ANSYS model was approximately 30 percent higher than the actual load at which cracking occurred. The FE model generally was considerably stiffer than the actual test slab. The top surface crack patterns at the final loads from the FE model corresponded well with the observed failure mode of the test slab.

2. The load-deflection response predicted by the ANSYS model was generally consistent with, but significantly stiffer than the actual load-deflection response. The FE model was stiffer than the test results in the linear and nonlinear range by approximately 68 and 30 percent respectively. The FE model underestimated the actual failure load of the test slab by only 8 percent.
3. The ANSYS model strain predictions matched the direction of the strain (tension or compression) seen in all experimental gauges for the 40 kip load level. The FE model predicted nominally higher strains at these locations for all but one gauge.

The results of this experimental study were also used to predict the number of load cycles required to deteriorate a bridge deck specimen once testing begins. Using a modified version of the fatigue life model developed by Matsui et al. (2001), reasonable testing times (i.e. 26 months) were predicted to deteriorate the deck panels when the panels are loaded above their cracking load (estimated to be 21 kips). That being said, if the applied load is below the cracking load of the slabs (i.e. 15 kips), testing times become impractical (i.e. 3,400 months). It may be possible to accelerate slab deterioration at lower load levels by pre-cracking the panels.

Recommendations for Future Research

Relative to the rolling wheel load tests to be conducted, it would seem essential in light of the fatigue life predictions done, to use as high a load as possible and/or to pre-crack the test slabs. Although not explored in this study, an alternate approach would be to reduce the slab thickness, which would decrease its capacity and fatigue life at a given load level. Notably, if the slab thickness was reduced to where a 15 kip load cracked the

slab, reasonable fatigue lives from a testing perspective would result. In any event, the results of this work can be used to determine load requirements to pre-crack existing slabs or for new slabs of reduced thickness.

Relative to further developing analytical ANSYS models of the deck panel to be used to support the test effort, it was evident that the Solid65 element exhibited significantly stiffer behavior than the experimental results. It is therefore recommended to investigate the reason behind this inconsistency. Factors suggested by past researchers that contribute to the ANSYS concrete model being too stiff include: the model's assumption of a perfect bond between the concrete and reinforcing steel and the exclusion of microcracks within the model. It is suggested to further investigate these factors as well as others that contribute to the Solid65 element being too stiff to properly model concrete so that a more accurate model can be developed. Note that, even with these shortcomings, these models were found to offer benefits in helping to interpret physical test behaviors.

REFERENCES

American Concrete Institute (ACI). (2008). “Building Code Requirements for Reinforced Concrete.” *ACI 318-08*, Farmington Hills, Mich.

American Institute of Steel Construction, Inc. (2005). *Steel Construction Manual*. United States of America: AISC.

ANSYS. (2008). ANSYS Manual Version 11.0, ANSYS Inc., Canonsburg, PA.

Bazant, Z. Email Interview. 2 Mar. 2012.

Desayi, P. ad Krishnan, S. (1954). “Equation for the Stress-Strain Curve of Concrete,” Journal of the American Concrete Institute, 61, pp. 345-350.

El-Gamal, S., El-Salakawy, E.F., and Benmokrane, B. (2005). “Behavior of Concrete Bridge Deck Slabs Reinforced with Fiber-Reinforced Polymer Bars Under Concentrated Loads,” ACI Structural Journal, Vol. 102, No. 5, pp. 727–735.

El-Gamal, S., El-Salakawy, E.F., and Benmokrane, B. (2007). “Influence of Reinforcement on the Behavior of Concrete Bridge Deck Slabs Reinforced with FRP Bars,” ASCE Journal of Composites for Construction. Vol. 11, No. 5, pp. 449-458.

El-Ragaby, A., El-Salakawy, E., and Benmokrane, B. (2007). “Fatigue Life Evaluation of Concrete Bridge Deck Slabs Reinforced with Glass FRP Composite Bars,” ASCE Journal of Composites for Construction. Vol. 11, No. 3, pp. 258-268.

Elstner, R.C., and Hognested, E. (1956). "Shearing Strength of Reinforced Concrete Slabs." ACI Journal, Proceedings Vol. 53, No. 1, pp. 29-58.

Emam, M. (1995). "Effect of Shear Strength on the Behavior of Slab-Column Connections Subjected to Monotonic and Cyclic Loading." Ph.D. Thesis, Civil Engineering Department, Cairo University.

Fenwick, R. C. and Dickson, A. R. (1989). “Slabs subjected to concentrated loading,” ACI Structural Journal (American Concrete Institute) 86:6 , pp. 672-678.

Fernando, E.G., Musani, D., Park, D., and Wenting, L. (2006). “Evaluation of Effects of Tire Size and Inflation Pressure on Tire Contact Stresses and Pavement Response,” Texas Transportation Institute.

Gebreyouhannes, E., Chijiwa, N., Fujiyama, C., and Maekawa, K. (2008). “Shear Fatigue Simulation of RC Beams Subjected to Fixed Pulsating and Moving Loads,” Journal of Advanced Concrete Technology, Vol. 6, No. 1, p. 215-226.

Graddy, J.C., Kim, J., Whitt, J.H., Burns, N.H., and Klingner, R.E. (2002). “Punching-Shear Behavior of Bridge Decks under Fatigue Loading,” ACI Structures Journal, 903, p. 257-266.

Hognested, E., Rachid. C., and Hanson, J.A. (1964). "Shear Strength of Reinforced Structural Lightweight Aggregate Concrete Slabs." Journal of the American Concrete Institute, Vol. 61, pp. 643-655.

Huang, Y., Adams, T.M., Pincheira, J.A. (2004) “Analysis of Life-Cycle Maintenance Strategies for Concrete Bridge Decks,” Journal of Bridge Engineering, Vol. 9, No. 3, pp. 250-258.

Ibrahim, A.M., and Mahmood, M.S. (2009). “ Finite Element Modeling of Reinforced Concrete Beams Strengthened with FRP Laminates,” European Journal of Scientific Research, Vol. 30, No. 4, pp. 526-541.

Kachlakev; D., Miller, T., Yim, S., Chansawat, K., and Potisuk, T. (2001). “Finite Element Modeling of Reinforced Concrete Structures Strengthened with FRP Laminates,” California Polytechnic State University, San Luis Obispo, CA and Oregon State University, Corvallis, OR for Oregon Department of Transportation.

Khanna, O.S.; Mufti, A. A.; and Bakht, B. (2000). “Experimental Investigation of the Role of Reinforcment in the Strength of Concrete Deck Slabs,” *Canadian Journal of Civil Engineering*, V. 27, pp. 475-480.

Kinnunen, S., and Nylander, H. (1960). "Punching of Concrete Slabs without Shear Reinforcement." Transactions of the Royal Institute of Technology, Stockholm, Sweden. No. 158.

Kuang, J.S. and Morley, C.T. (1992). “Punching Shear Behavior of Restrained Reinforced Concrete Slabs,” ACI Structural Journal, V. 89, No. 1, 1992, pp. 13-19.

Marzouk, H., and Hussien, A. (1991). "Punching Shear Analysis of Restrained High Strength Concrete Slabs." Canadian Journal of Civil Engineering, Vol. 18, pp. 954-963.

Matsui, S., Tokai, D., Higashiyama, H., and Mizukoshi, M. (2001). "Fatigue Durability of Fiber-Reinforced Concrete Decks under Running Wheel Load," Proceedings: 3rd International Conference on Concrete under Severe Conditions, University of British Columbia, Vancouver, Canada, p. 982–991.

Mufti, A. A., and Newhook, P. J. (1998). "Punching Shear Strength of Restrained Concrete Bridge Deck Slabs," *ACI Structural Journal*, V. 95, No. 4, pp. 375-381.

Newhook, J. P. (1997). "The Behavior of Steel-Free Concrete Bridge Deck Slabs Under Static Loading Conditions," PhD thesis, DalTech, Dalhousie University, Halifax, Nova Scotia, Canada.

Pan, T., Shi, X., and Stephens, J. (2007). "Validation of Rehabilitation Strategies to Extend the Service life of Concrete Bridge Decks, Proposal" Western Transportation Institute.

Perdikaris, P.C., and Beim, S. (1988). "RC Bridge Decks under Pulsating and Moving Load," Journal of Structural Engineering, 1143, p. 591–607.

Perdikaris, P.C., Beim, S.R., and Bousias, S.N. (1989). "Slab Continuity Effect on Ultimate and Fatigue Strength of Reinforced Concrete Bridge Deck Models," ACI Structural Journal, 86(4) p. 483-491.

Petrou, M., Perdikaris P. C., and Wang A. (1994). "Fatigue Behavior of Non-composite Reinforced Concrete Bridge Deck Models," *Transportation Research Record 1460*, TRB, National Research Council, Washington, D.C., pp.73-80.

Rahim A., Jansen, D., and Abo-Shadi, N. (2006). "Concrete Bridge Deck Crack Sealing: An Overview of Research". Final Report submitted to California Department of Transportation.

Salim, W. and Sebastian, W. M. (2003). "Punching shear failure in reinforced concrete slabs with compressive membrane action," ACI Structural Journal 100:4 , pp. 471-479.

Stordahl, A. (2009). "Validation of Rehabilitation Strategies to Extend the Service Life of Concrete Bridge Decks," Professional Paper, Montana State University, Bozeman, Montana.

Tavarez, F.A. (2001). "Simulation of Behavior of Composite Grid Reinforced Concrete Beams Using Explicit Finite Element Methods," Master's Thesis, University of Wisconsin-Madison, Madison, Wisconsin.

Willam, K. J., and Warnke, E. D. (1975). "Constitutive Model for the Triaxial Behavior of Concrete," Proceedings, International Association for Bridge and Structural Engineering, Vol. 19, ISMES, Bergamo, Italy, p. 174.

Wolanski, A.J. (2004). “Flexural Behavior of Reinforced and Pre-stressed Concrete Beams Using Finite Element Analysis,” Master’s Thesis, Marquette University, Milwaukee, Wisconsin.

APPENDIX A:

LABORATORY TEST SPECIFICATIONS

CUSTOMER			TICKET NO.	LOAD NO.	PLANT
MSU - Western Transportation Ins			46632	82087	4
TRUCK	TICKET NUM	TICKET ID	TIME	DATE	
9964	46632	52623	7:32	6/7/2010	
LOAD SIZE	MIX CODE				
2.50 yd	11650001				

MATERIAL	DESIGN QTY	REQUIRED	BATCHED	VAR	% VAR	% MOISTURE	ACTUAL WAT
# 4 Coarse	1639 lb	4098 lb	4110.0	12	0.29%		
Concrete Sand	1148 lb	2985 lb	2960.0	-25	-0.84%	4.00%	13.64 gl
Type I/II	521 lb	1302.5 lb	1290.0	-12.5	-0.96%		
Class F Ash	174 lb	435 lb	425.0	-10	-2.30%		
Air Admixture	1.50 oz	3.75 oz	0.0	-3.75	-100.00%		
Water Reducer	33.00 oz	82.50 oz	84.0	1.5	1.82%		
Water	30.00 gl	61.24 gl	61.0	-0.24	-0.39%		61.00 gl

LOAD TOTAL:	9300 lb				
DESIGN W/C:	0.360				
WATER/CEMENT:	0.365T				
DESIGN WATER:	75.0 gl				
ACTUAL WATER:	74.6 gl	TO ADD:	0.4 gl	WATER IN TRUCK:	0.0 gl
ADJUST WATER	none				
SLUMP:	3.00 "				

LOAD COMPLETED LOAD TIME: 03:01

Figure 45: Concrete Mix Design

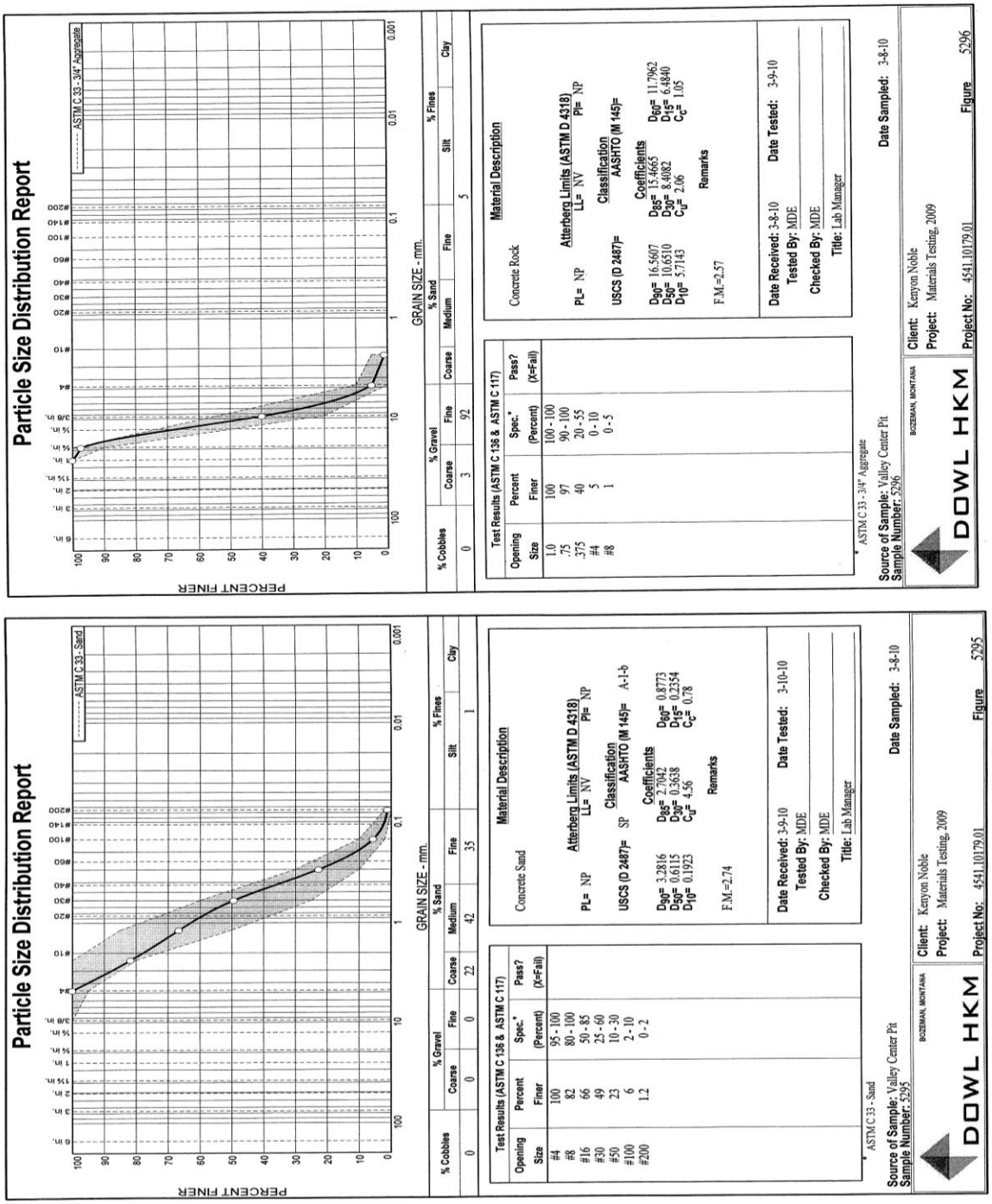

Figure 46: Distribution Charts for Coarse and Fine Aggregate in Concrete Mix

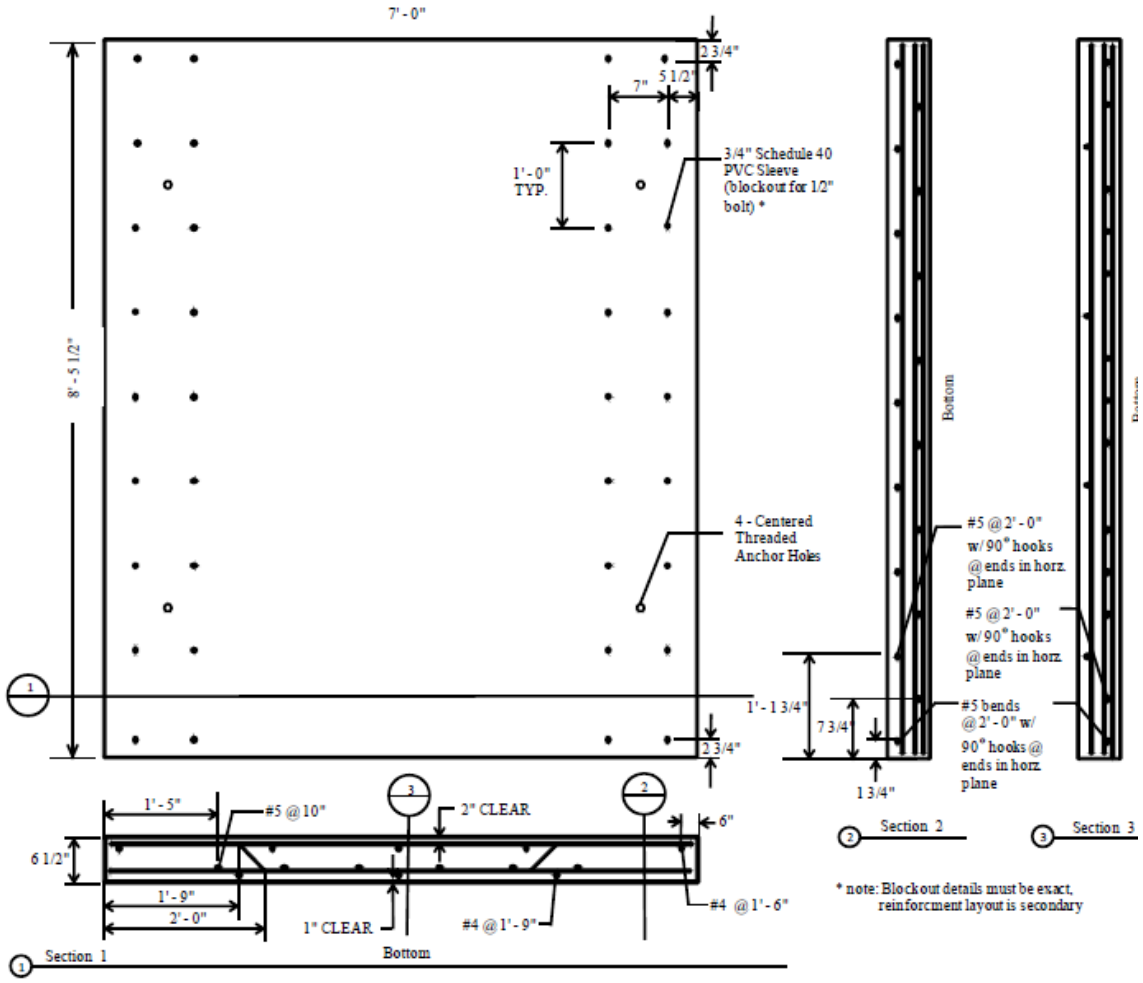

Figure 47: Test Specimen Detail

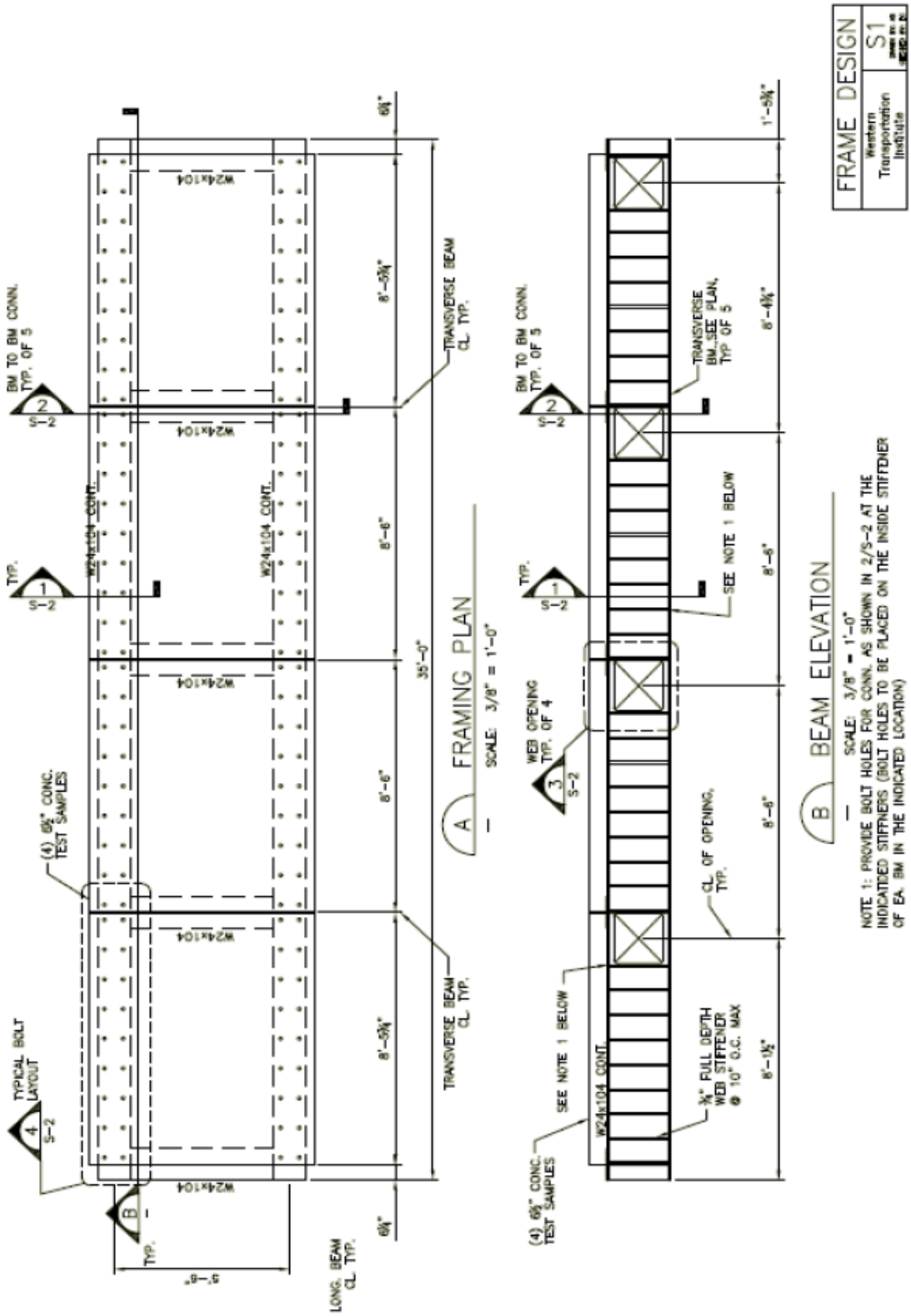

Figure 48: Schematic of Support Frame (Part 1)

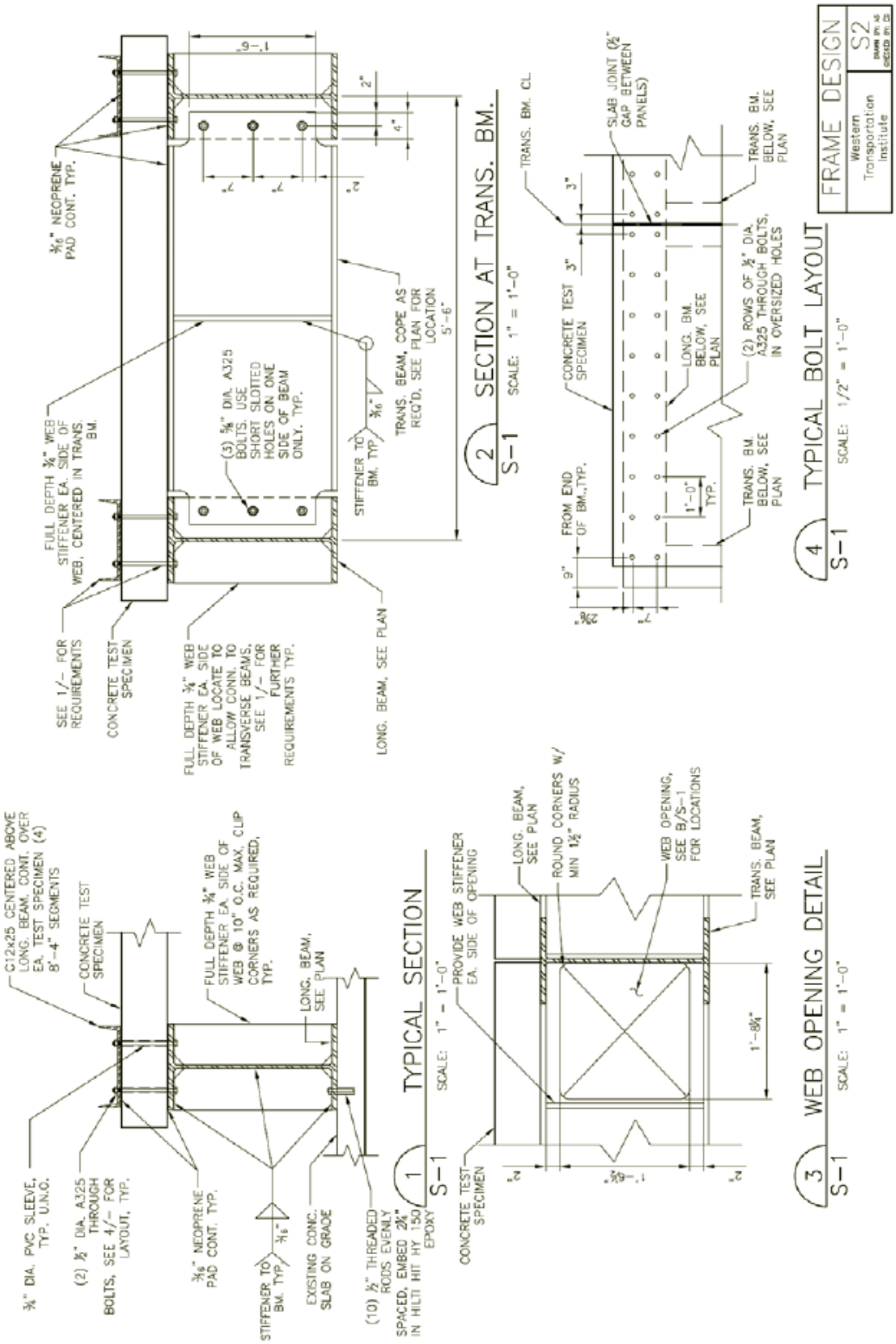

Figure 49: Schematic of Support Frame (Part 2)